

The ectonucleotidase CD39 identifies tumor-reactive CD8⁺ T cells predictive of immune checkpoint blockade efficacy in human lung cancer

Highlights

- CD39⁺ CD8⁺ T cells express features of exhaustion and tumor reactivity
- CD39 expression enriches for CD8⁺ TCRs with tumor reactivity
- CD39 expression on CD8⁺ T cells is non-redundant to tumor-based biomarkers
- CD39⁺ CD8⁺ T cells are predictive of benefit from ICB

Authors

Andrew Chow, Fathema Z. Uddin, Michael Liu, ..., Jedd D. Wolchok, Taha Merghoub, Charles M. Rudin

Correspondence

chowa1@mskcc.org (A.C.), tmerghoub@med.cornell.edu (T.M.), rudinc@mskcc.org (C.M.R.)

In brief

Factors predicting benefit of immune checkpoint blockade (ICB) are needed. Here, Chow et al. demonstrate that CD39 expression marks tumor-reactive CD8⁺ T cells. High baseline levels of CD39⁺ CD8⁺ T cells are associated with ICB efficacy in lung cancer. Thus, CD39 is a potential tumor-extrinsic biomarker for guiding cancer management.



Article

The ectonucleotidase CD39 identifies tumor-reactive CD8⁺ T cells predictive of immune checkpoint blockade efficacy in human lung cancer

Andrew Chow,^{1,2,3,*} Fathema Z. Uddin,^{1,18} Michael Liu,^{1,18} Anton Dobrin,^{4,5,18} Barzin Y. Nabet,⁶ Levi Mangarin,² Yonit Lavin,¹ Hira Rizvi,^{7,15} Sam E. Tischfield,⁸ Alvaro Quintanal-Villalonga,¹ Joseph M. Chan,¹ Nisargbhai Shah,¹ Viola Allaj,¹ Parvathy Manoj,¹ Marissa Mattar,⁹ Maximiliano Meneses,⁹ Rebecca Landau,⁹ Mariana Ward,⁹ Amanda Kulick,⁹ Charlene Kwong,⁹ Matthew Wierzbicki,⁹ Jessica Yavner,⁹ Jacklynn Egger,⁷ Shweta S. Chavan,⁸ Abigail Farillas,¹ Aliya Holland,² Harsha Sridhar,¹ Metamia Ciampricotti,¹ Daniel Hirschhorn,² Xiangnan Guan,⁶ Allison L. Richards,⁸ Glenn Heller,¹⁰ Jorge Mansilla-Soto,⁴ Michel Sadelain,^{3,4} Christopher A. Klebanoff,^{3,4,11,12,13} Matthew D. Hellmann,^{1,3,13,15} Triparna Sen,^{1,16} Elisa de Stanchina,⁹ Jedd D. Wolchok,^{2,3,12,13,17,19,20} Taha Merghoub,^{2,3,12,13,17,19,20,*} and Charles M. Rudin^{1,3,7,14,19,20,21,*}

¹Thoracic Oncology Service, Department of Medicine, Memorial Sloan Kettering Cancer Center, New York, NY, USA

²Ludwig Collaborative and Swim Across America Laboratory, Memorial Sloan Kettering Cancer Center, New York, NY, USA

³Department of Medicine, Weill Cornell Medical College, New York, NY, USA

⁴Center for Cell Engineering, Memorial Sloan Kettering Cancer Center, New York, NY, USA

⁵Louis V. Gerstner, Jr. Graduate School of Biomedical Sciences, Memorial Sloan Kettering Cancer Center, New York, NY, USA

⁶Department of Oncology Biomarker Development, Genentech, South San Francisco, CA, USA

⁷Druckenmiller Center for Lung Cancer Research, Memorial Sloan Kettering Cancer Center, New York, NY, USA

⁸Marie-Josée and Henry R. Kravis Center for Molecular Oncology, Memorial Sloan Kettering Cancer Center, New York, NY, USA

⁹Antitumor Assessment Core, Memorial Sloan Kettering Cancer Center, New York, NY, USA

¹⁰Department of Epidemiology & Biostatistics, Memorial Sloan Kettering Cancer Center, New York, NY, USA

¹¹Breast Medicine Service, Department of Medicine, Memorial Sloan Kettering Cancer Center, New York, NY, USA

¹²Human Oncology and Pathogenesis Program, Memorial Sloan Kettering Cancer Center, New York, NY, USA

¹³Parker Institute for Cancer Immunotherapy, Memorial Sloan Kettering Cancer Center, New York, NY, USA

¹⁴Molecular Pharmacology Program, Memorial Sloan Kettering Cancer Center, New York, NY, USA

¹⁵Present address: Oncology R&D, Astra-Zeneca, USA

¹⁶Present address: Tisch Cancer Institute, Icahn School of Medicine at Mount Sinai, New York, USA

¹⁷Present address: Sandra and Edward Meyer Cancer Center, Weill Cornell Medicine, New York, NY, USA

¹⁸These authors contributed equally

¹⁹These authors contributed equally

²⁰Senior author

²¹Lead contact

*Correspondence: chowa1@mskcc.org (A.C.), tmerghoub@med.cornell.edu (T.M.), rudinc@mskcc.org (C.M.R.)

<https://doi.org/10.1016/j.immuni.2022.12.001>

SUMMARY

Improved identification of anti-tumor T cells is needed to advance cancer immunotherapies. CD39 expression is a promising surrogate of tumor-reactive CD8⁺ T cells. Here, we comprehensively profiled CD39 expression in human lung cancer. CD39 expression enriched for CD8⁺ T cells with features of exhaustion, tumor reactivity, and clonal expansion. Flow cytometry of 440 lung cancer biospecimens revealed weak association between CD39⁺ CD8⁺ T cells and tumoral features, such as programmed death-ligand 1 (PD-L1), tumor mutation burden, and driver mutations. Immune checkpoint blockade (ICB), but not cytotoxic chemotherapy, increased intratumoral CD39⁺ CD8⁺ T cells. Higher baseline frequency of CD39⁺ CD8⁺ T cells conferred improved clinical outcomes from ICB therapy. Furthermore, a gene signature of CD39⁺ CD8⁺ T cells predicted benefit from ICB, but not chemotherapy, in a phase III clinical trial of non-small cell lung cancer. These findings highlight CD39 as a proxy of tumor-reactive CD8⁺ T cells in human lung cancer.

INTRODUCTION

Lung cancer is the leading cause of cancer death in the world. Immune checkpoint blockade (ICB) has been a remarkable clin-

ical advancement in the treatment of lung cancer; however, most patients do not respond to ICB therapy, and many of those who initially responded eventually develop recurrent and progressive disease.^{1,2} While programmed death-ligand 1 (PD-L1) on tumor



cells and tumor mutation burden (TMB) have been validated as predictors of benefit from ICB in lung cancer,^{3,4} there is an opportunity to further refine these biomarkers by incorporating features of CD8⁺ T cells, which are critical mediators of ICB efficacy.

Total CD8⁺ T cell content alone is not a reliable predictor of clinical benefit from ICB.^{5–9} Part of the reason for this lack of predictive benefit is that a large and variable proportion of CD8⁺ T cells in the tumor microenvironment is bystander T cells that lack tumor reactivity.^{10,11} CD8⁺ T cells that express CD39 are enriched for features of a clonal, proliferative lymphocyte population that express high levels of activation/exhaustion (e.g., programmed cell death-1 [PD-1]) and cytotoxicity (e.g., granzyme B) markers.^{2,11–14} Moreover, CD39 is highly expressed on empirically defined neoantigen- and tumor-associated-antigen-reactive T cells in lung cancer and melanoma.^{15–18} In this study, we characterized human CD39⁺ CD8⁺ T cells in lung cancer with single-cell sequencing, T cell receptor (TCR) cloning, and tumor co-culture assays. Furthermore, to investigate the utility of CD39 as a biomarker in ICB, we evaluated the tumoral features associated with %CD39⁺ among CD8⁺ T cells from 440 clinical samples of human lung cancer and investigated whether the baseline abundance of CD39⁺ CD8⁺ T cells was associated with ICB efficacy in patients with lung cancer.

RESULTS

CD8⁺ T cells with high expression of CD39 are enriched for features of exhaustion, tumor reactivity, and clonal expansion

To characterize CD8⁺ T cells expressing the protein CD39, we sorted CD3⁺ T cells from four non-small cell lung cancer (NSCLC) biospecimens and performed single-cell cellular indexing of transcriptomes and epitopes (CITE)/RNA/TCR sequencing.¹⁹ The four NSCLC samples comprised a range of histologies (e.g., adenocarcinoma and squamous), driver mutations (*KRAS* and *EGFR*), stages (e.g., early and metastatic), and anatomic sites (e.g., lung, pleural fluid, and brain) (Table S1). None of these patients had received prior ICB at the time of sample collection. After coarse clustering, we visualized distinct clusters of regulatory T cells, CD4⁺ T cells, CD8⁺ T cells, and an additional T cell not otherwise specified (NOS) cluster (Figure 1A; Table S2A). We focused our subsequent analyses on CD8⁺ T cells, since this subset has the greatest known contribution to anti-tumor immunity. The 896 single CD8⁺ T cells that passed quality control were divided by CD39 protein expression (assessed by oligo-tagged anti-CD39 antibody) into high (hi), intermediate (int), and negative (neg) groups. Transcriptional dropout is a well-known limitation of the single-cell RNA-seq, and oligonucleotide-tagged antibodies to surface molecules (e.g., CITE-seq) represent a strategy to overcome this hurdle.²⁰ Concordantly, CITE-seq detected the protein expression of CD39 and other activation markers in many cells in which transcriptional expression was absent (Figure S1A). Genes that were differentially expressed by CD39^{hi} CD8⁺ T cells included the exhaustion marker *LAYN*, tissue residence marker *ITGAE* (encoding CD103), and the activation markers *CXCL13*, *GNLY*, *HLADRA*, and *VCAM1* (Table S2B). CD39^{hi} CD8⁺ T cells showed the highest gene expression of *ENTPD1* (encoding CD39),

PDCD1 (encoding PD-1), *ITGAE*, *CXCL13*, *TNFRSF4* (encoding OX-40), *HAVCR2* (encoding TIM-3), and *LAG3*, which are features of tumor-reactive CD8⁺ T cells (Figure S1B).²¹ Assessment of extracellular protein expression by CITE-seq revealed that CD39^{hi} CD8⁺ T cells across the four samples consistently expressed the highest protein PD-1, CD103, OX40, 4-1BB, and LAG-3 (Figure 1B). Concordantly, CD39^{hi} CD8⁺ T cells expressed the highest transcriptomic signature score for T cell exhaustion²² and tumor reactivity²¹ and the lowest score for progenitor exhausted CD8⁺ T cells^{23,24} (Figures 1C, 1D, and S1C; Table S3).

We next evaluated whether the gene expression profiles of CD39^{hi} CD8⁺ T cells in our dataset overlapped with previously reported gene signatures of CD8⁺ T cells that were reactive to tumor-associated or viral-associated antigens.^{15,16} CD39^{hi} CD8⁺ T cells in our dataset indeed expressed the highest “tumor-specific” and “mutation-associated neoantigen-tumor-infiltrating lymphocyte (MANA-TIL)” signature scores and lowest “virus-specific” and “influenza” signatures (Figures 1E, 1F, S1D, and S1E). CD39^{hi} CD8⁺ T cells also expressed the highest proliferation score, and both CD39^{int} and CD39^{hi} CD8⁺ T cells comprised a higher clonal proportion among all CD8⁺ T cells (Figures 1G and 1H). Thus, our single-cell CITE/RNA/TCR sequencing demonstrated that CD39^{hi} CD8⁺ T cells express features of exhaustion, tumor reactivity, and clonal expansion.

CD39⁺ CD8⁺ T cells are enriched for tumor reactivity

We developed patient-derived xenograft (PDX) models from two of the patients from which we obtained single-cell CITE/RNA/TCR sequencing—MSK 1087 and 1111. We sought to empirically determine whether CD39 expression enriched for CD8⁺ T cells that were tumor reactive. In order to circumvent the potential confounder of differential degrees of T cell exhaustion among CD39^{hi}, CD39^{int}, and CD39^{neg} CD8⁺ T cells, we cloned TCR α and TCR β sequences from CD8⁺ T cells from MSK 1087 and 1111 and retrovirally transduced them into healthy donor PBMCs that underwent CRISPR-Cas9 editing to disrupt the endogenous TCR α and TCR β constant chain sequences (Figure 2A; Table S4). CRISPR-Cas9 editing of the endogenous TCR constant chains led to efficient endogenous TCR disruption, as indicated by >90% decrease in surface CD3 expression (Figure 2B). Viral transduction (marked by truncated EGFR [EGFRt] expression) with a donor TCR restored CD3 expression in a subset of the T cells. TCR transduction with an NY-ESO1 TCR mediated TCR reactivity (as assessed by 4-1BB upregulation in the EGFRt⁺ population¹⁶) against a lung cancer cell line H522 (human leukocyte antigen [HLA]-A*02:01) that was transduced to overexpress NY-ESO1 (H522-NY-ESO1) (Figure 2B). Across the two PDX models, 6 of 39 tested TCRs were tumor reactive (Figures 2C–2E). Also, 33%, 15.8%, and 7.1% of tested CD39^{hi}, CD39^{int}, and CD39^{neg} CD8⁺ TCRs mediated tumor reactivity, respectively (Figure 2F). Thus, CD39 expression on CD8⁺ T cells enriches for the TCRs that can recognize tumor antigens.

CD39 expression is dependent on antigen-specific TCR engagement

Murine CD8⁺ T cells increase CD39 expression after polyclonal and antigen-specific activation, but the kinetics is distinct from that of other activation/exhaustion markers, such as

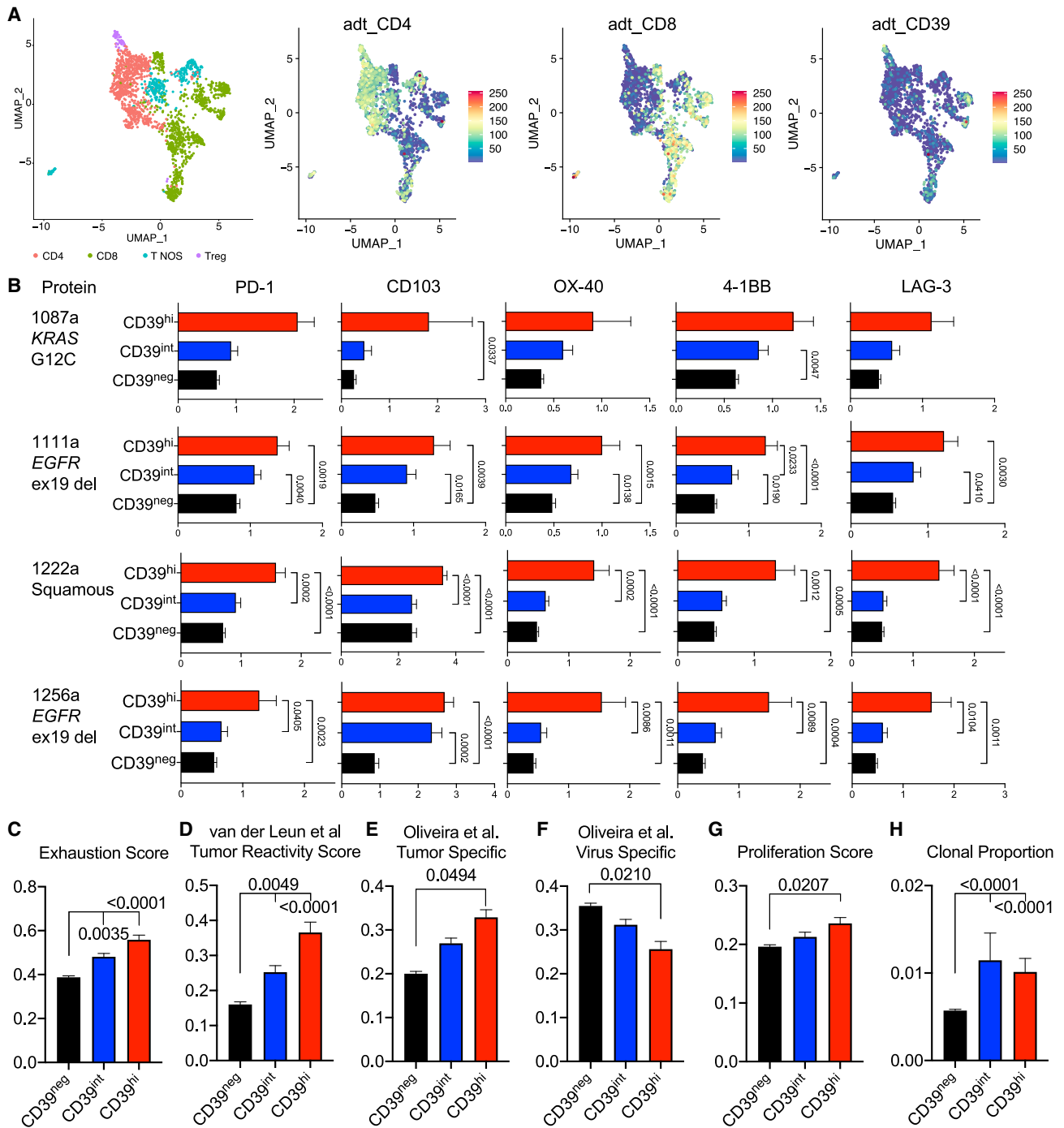


Figure 1. Single-cell CITE/RNA/TCR sequencing reveals that CD39^{hi} CD8⁺ T cells are enriched for features of exhaustion, tumor reactivity, and clonal proliferation in human lung cancer

(A) UMAP of sorted CD3⁺ T cells from four patients with lung cancer (Table S1). Clusters are annotated on left panel. Surface levels of CD4, CD8, and CD39 as assessed by CITE-seq antibody-derived tags (adt) are depicted in right three panels.

(B) Levels of various proteins (column) across the four samples (row) as determined by CITE-seq adt levels.

(C–G) Scaled scores for exhaustion, tumor reactivity, tumor specific, virus specific, and proliferation gene signatures (Table S4).

(H) Clonal proportion among CD8⁺ T cells of clonotypes that were categorized by mean CD39 expression. Error bars indicate SEM.

Statistical significance was determined with two-way ANOVA with Tukey's multiple comparisons test, and p value is indicated if < 0.05.

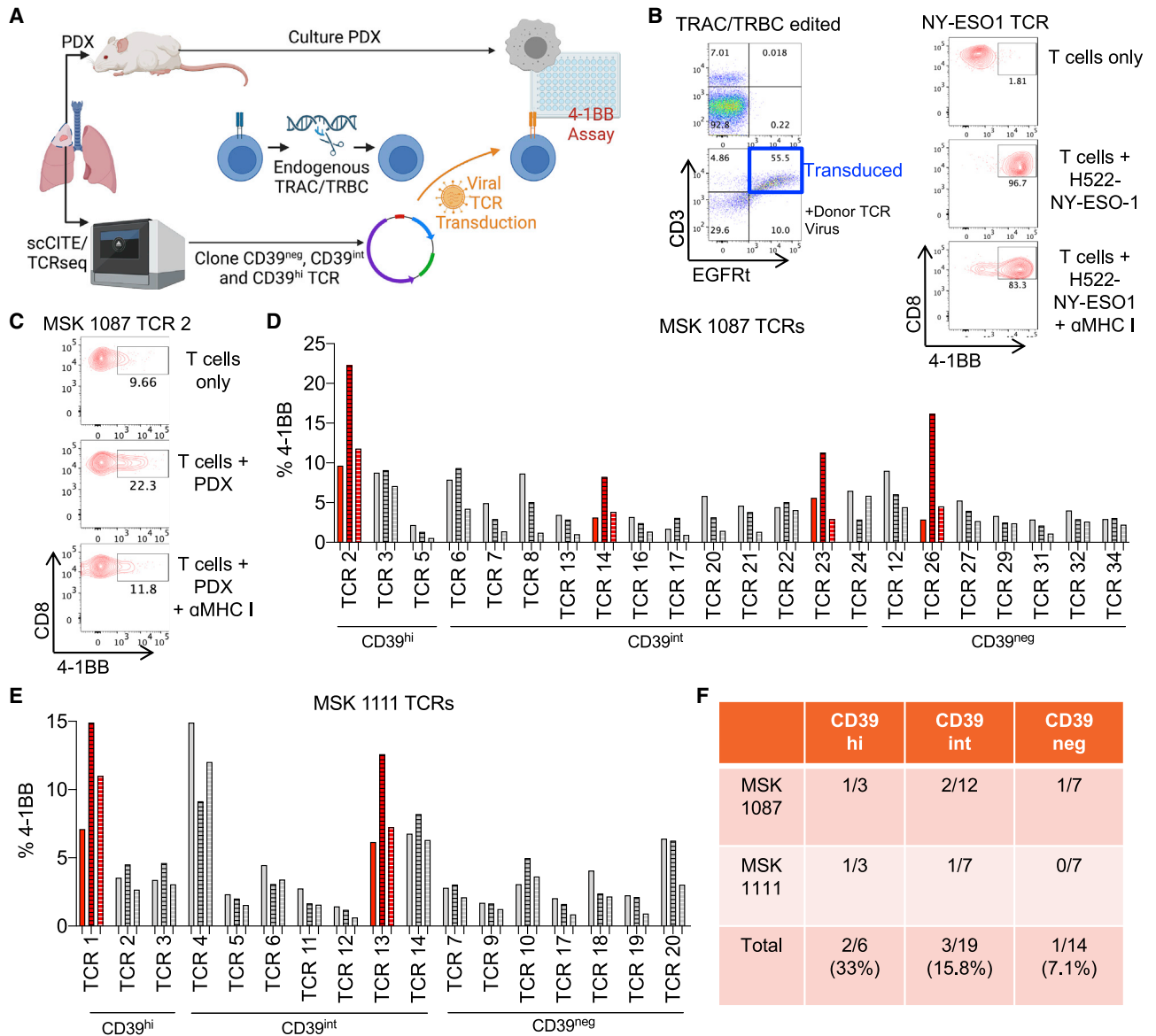


Figure 2. CD39 enriches for tumor-reactive TCRs in lung cancer

(A) Schematic outlining the parallel derivation of a patient-derived xenograft for MSK 1087 and MSK 1111 and cloning and transduction of candidate CD39^{neg}, CD39^{int}, and CD39^{hi} TCRs into healthy donor CD8⁺ T cells deleted for endogenous TCRs. The cultured PDX cells and transduced donor CD8⁺ T cells were co-cultured for 24 h, and 4-1BB expression was evaluated on transduced T cells.

(B) Flow cytometry plots of CD3 and EGFRt expression on untransduced TRAC/TRBC-edited CD8⁺ T (left top panel) or TRAC/TRBC-edited CD8⁺ T transduced with donor NY-ESO1 TCR (left bottom panel, blue box indicates transduced population). Flow cytometry plots of CD8⁺ and 4-1BB expression for NY-ESO1 TCR-transduced T cells that were cultured alone (right top panel), with H522-NY-ESO1 (right middle), or H522-NY-ESO1 with anti-MHC I (right lower).

(C) Flow cytometry plots of CD8⁺ and 4-1BB expression for MSK 1087 TCR 2-transduced T cells that were cultured alone (top panel), with MSK 1087 PDX (middle), or MSK 1087a PDX with anti-MHC I (lower).

(D) Bar plots of %4-1BB among EGFRt⁺ transduced T cells that were cultured alone (left solid bar in each series of three bars), with MSK 1087 PDX cells (middle bar with black dash), or with MSK 1087 PDX cells treated and anti-MHC I (right bar with white dash). Red bars indicate TCRs that are tumor-reactive (the %4-1BB level for the culture with PDX tumor cells is $\geq 5\%$ higher than the culture with only T cells).

(E) Bar plots of %4-1BB among EGFRt⁺ transduced T cells that were cultured alone (left solid bar), with MSK 1111 PDX cells (middle bar with black dash), or with MSK 1111 PDX cells treated and anti-MHC I (right bar with white dash). Red bars indicate TCRs that are tumor reactive.

(F) Tabulation of reactive TCRs after co-culture with patient-matched PDX tumor cells.

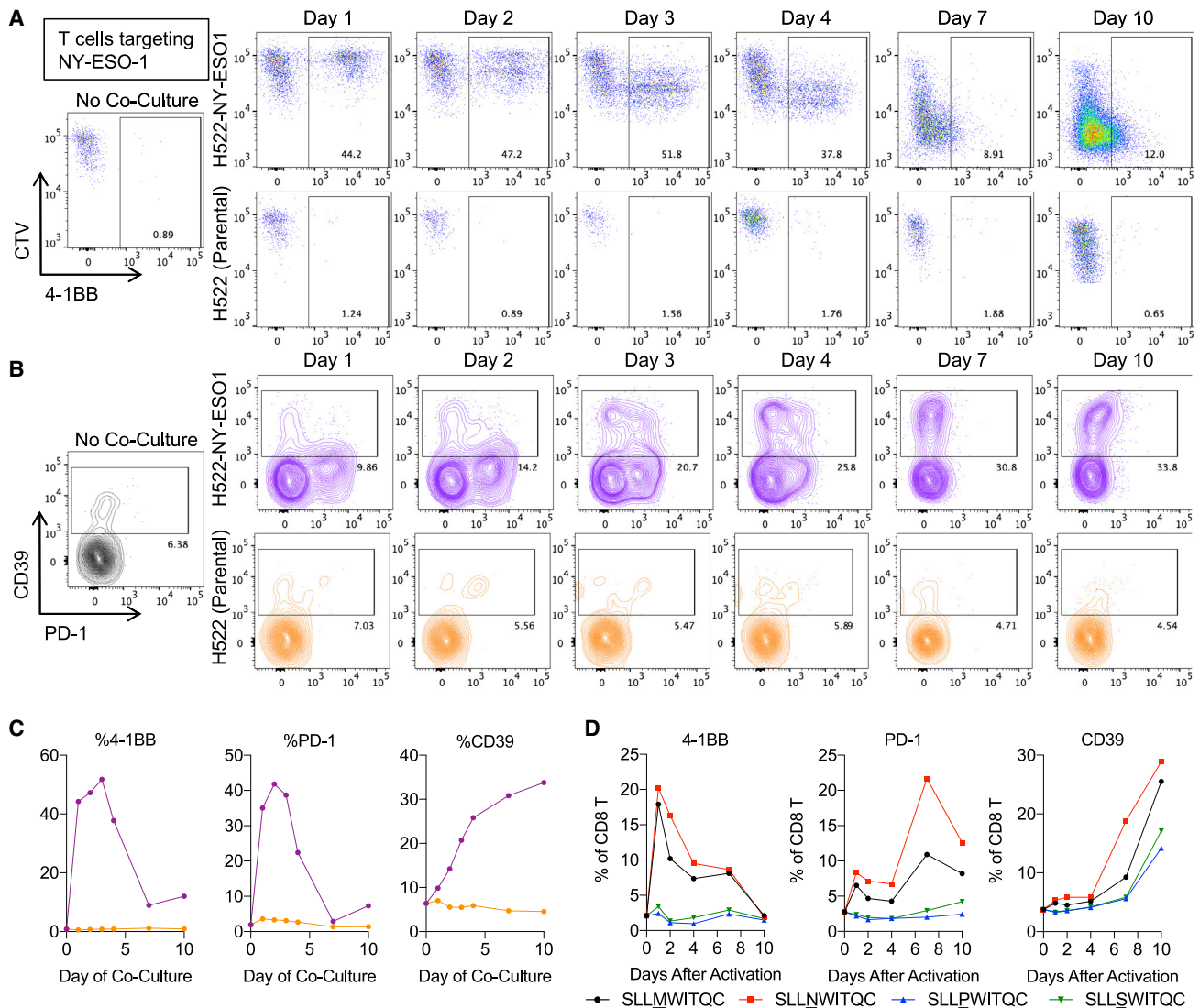


Figure 3. CD39 is durably expressed after antigen-specific stimulation

(A) Flow cytometry plots of CTV and 4-1BB levels of NY-ESO1-specific CD8⁺ T cells that were cultured with no tumor cells (far left plot), H522-NY-ESO1 (top row of plots), or parental H522 (bottom row of plots) for the indicated number of days.

(B) Flow cytometry plots of CD39 and PD-1 levels of NY-ESO1-specific CD8⁺ T cells that were cultured with no tumor cells (far left plot), H522-NY-ESO1 (top row of purple plots), or parental H522 (bottom row of orange plots) for the indicated number of days.

(C) Levels of %4-1BB⁺, %PD-1⁺, or %CD39⁺ among NY-ESO1-specific CD8⁺ T cells during co-culture with H522-NY-ESO1 (purple line) or parental H522 (orange line).

(D) Levels of %4-1BB⁺, %PD-1⁺, or %CD39⁺ among NY-ESO1-specific CD8⁺ T cells during co-culture with parental H522 pulsed with the NY-ESO1 altered peptide ligands SLLM<u>W</u>ITQC (black line), SLLN<u>W</u>ITQC (red line), SLLP<u>W</u>ITQC (blue line), or SLLS<u>W</u>ITQC (green line).

phosphatidylserine, CD44, and PD-1.²⁵ Whereas phosphatidylserine, CD44, and PD-1 peak quickly and attenuate after activation, CD39 levels are slower to rise and persist for a long period on the cell surface. Polyclonal activation of human CD8⁺ T cells show the same kinetic distinction between CD39 and the other activation/exhaustion markers. We next profiled the expression of CD39 on human CD8⁺ T cells during the course of antigen-specific T cell stimulation. To evaluate this, we utilized commercially available CD8⁺ T cells recognizing NY-ESO1 presented on HLA-A*02:01 (73.74% enrichment by tetramer analysis). In contrast to TCR-transduced cells, these cells underwent peptide

stimulation through an endogenous TCR, which more closely approximated antigen-experienced T cells that have completed priming in the secondary lymphoid organs. Moreover, placing these post-primed cells into co-culture with tumor targets more closely approximated the context of T cell-tumor cell encounter in the tumor microenvironment, where CD39 is most upregulated (see below Figure S4). Co-culture with H522-NY-ESO1, but not the parental H522 cell line, induced CD8⁺ T cell proliferation (indicated by CellTrace Violet dilution) and rapid expression of 4-1BB and PD-1 (Figures 3A–3C). CD39 expression increased more slowly over the course of a 10-day

co-culture and did not attenuate as quickly as 4-1BB and PD-1 (Figures 3A–3C). Thus, although frequently co-expressed (Figure 1B), there are differences in the kinetics of expression between CD39, PD-1, and 4-1BB after antigen stimulation.

To further characterize how antigen-specific stimulation culminates in CD39 expression, we utilized the same CD8⁺ T cells that were enriched for NY-ESO1 reactivity and placed them into co-culture with parental H522 cells that were pulsed with the NY-ESO1 peptide SLLMWITQC at varying concentrations. Whereas the 10 µg/mL concentration of peptide induced 4-1BB and PD-1 reactivity, there was minimal upregulation of 4-1BB and PD-1 at either 0.1 or 1 µg/mL concentrations (Figures S2A and S2B). All three peptide concentrations resulted in increased expression of CD39 by 10 days after coculture, and the highest CD39 expression was observed at the 10 µg/mL concentration (Figure S2C). Therefore, antigen-specific TCR stimulation induces CD39 expression in a time-dependent and antigen-density-dependent manner.

Altered peptide ligands (APLs) are single amino acid changes in the TCR-facing surface of the peptide, which confer differences in TCR signal strength.²⁶ Since the M4 position of the NY-ESO1 peptide SLLMWITQC is essential for TCR binding,²⁷ we generated the APLs SLLNWITQC, SLLPWITQC, and SLLSWITQC. As assessed by 4-1BB and PD-1 increases, the amino acid change from methionine (M) to asparagine (N) resulted in mildly increased TCR avidity, whereas the change to proline (P) or serine (S) substantially reduced TCR avidity (Figures 2D and S2A–S2C). For all four peptides, CD39 expression increased over time during co-culture, and the degree of increase matched the rank order of observed TCR avidity (SLLNWITQC > SLLMWITQC > SLLSWITQC > SLLPWITQC). Hence, we observed that the expression of CD39 on human CD8⁺ T cells is dependent on TCR signal strength.

CD39 expression on CD8⁺ T cells is a non-redundant biomarker

We assessed CD39, Tim-3, 4-1BB, and PD-1 expressions by flow cytometry to compare their relative staining resolution, as defined by the separation of the positive and negative populations. FACS-based detection of CD39 consistently yielded a higher resolution compared with the other three markers (Figure 4A). The enhanced resolution of CD39, compared with those of 4-1BB and PD-1, was consistent with the observed, more durable expression of CD39 in CD8⁺ T cells (Figures 3A–3C; Chow et al.²⁵). Due to the staining resolution of the CD39 marker and its association with tumor reactivity, we utilized CD39 expression on CD8⁺ T cells to estimate the frequency of tumor-reactive CD8⁺ T cells in lung cancer clinical samples. From August 2018 to September 2021, we evaluated 440 fresh lung cancer clinical specimens by flow cytometry for CD39 expression on CD8⁺ T cells. These biospecimens ranged across stages (I–IV) and lung cancer subtypes (lung adenocarcinoma, squamous cell cancer, and small cell lung cancer [SCLC]) (Table S5A). The median frequency of CD8⁺ T cells was 13.0% (of CD45⁺), and median %CD39⁺ was 15.65% (of CD8⁺ T cells), and these were utilized as cutoffs in the study. On univariate analysis, CD39 expression on CD8⁺ T cells had a weak correlation with total CD8⁺ T cells, smoking history, TMB, and PD-L1 (Figures S3A–S3D). Since TMB ≥ 10 mutations/Mb and PD-

L1 ≥ 50% represent subgroups with favorable clinical outcomes from ICB therapy,^{3,4} we assessed the frequency of CD39-expressing cells in these subpopulations. When divided into four subgroups by PD-L1 and TMB expression, the %CD39⁺ among tumor CD8⁺ T cells from the two TMB ≥ 10 mutations/Mb subgroups (both PD-L1 <50% and ≥50%) was nearly 2-fold higher than that from the TMB < 10% and PD-L1 < 50% subgroups (Figure S3E). By contrast, the proportion of CD8⁺ T cells (Figure S3F) showed less variation. There was largely no association of CD39 expression on CD8⁺ T cells with lung cancer stage, with the exception of a reduction in stage IVA tumors (Figure S3G). This was consistent with reduced CD39 expression on CD8⁺ T cells in pleural fluid and pleural metastases biospecimens relative to the lung biospecimens (Figure S3H). Due to the more fluid nature of this microenvironment, the stability of tumor cell-CD8⁺ T cell interaction may be reduced, resulting in reduced CD39 expression. Pleural and peritoneal cavities are immunosuppressed microenvironments due to the presence of Tim-4⁺ cavity-resident macrophages,²⁵ and this may contribute to the reduced proportion of CD8⁺ T cells expressing CD39 in these anatomic compartments.

%CD39⁺ on CD8⁺ T cells showed two patterns of expression among the lung cancer subtypes. *ALK* fusion, *ROS1* fusion, *RET* fusion, *MET* exon 14 fusion, *BRAF* V600E, and *EGFR* mutant (except exon 20 insertion) lung adenocarcinomas, which are not associated with tobacco use, had below median CD39 expression on CD8⁺ T cells (Figure 4B; Table S5B). The reduced %CD39⁺ on CD8⁺ T cells from *EGFR* mutant lung cancer tumors was in line with a prior report.¹¹ By contrast, CD39 expression on lung adenocarcinomas with *KRAS* G12C, G12D, and G12V mutations were above median. Other *KRAS* mutations—including G12A, G12R, G12S, G13C, G13D, Q61H, and Q61R, which are known to be oncogenic per OncoKB²⁸—were also associated with above median %CD39⁺ on CD8⁺ T cells. The median proportion of CD39⁺ CD8⁺ T cells in adenocarcinomas with an *ERBB2* (HER2) driver mutation and squamous lung cancers also had above median CD39 levels on CD8⁺ T cells. These findings are consistent with *KRAS* and squamous lung cancers being associated with tobacco use, which are correlated with a higher number of tumor mutations and neoantigens to which CD8⁺ T cells can react. SCLC is also associated with tobacco use and high TMB levels (Figure S3I); yet, this subtype of lung cancer only had a median CD39 level of 14.0%. This may partially explain the relatively low level of additive efficacy of ICB in SCLC^{29,30} and may be related to reduced MHC I expression on SCLC cells,^{31,32} which would impair antigen-induced CD39 expression (Figure 3). Even among the lung cancer subtypes with higher CD39 expression, there was a wide range of CD39 levels (Figure 4B), suggesting that even for a given driver mutation, there is substantial heterogeneity in tumor-reactive CD8⁺ T cell immunosurveillance. Total CD8⁺ T cell infiltration, TMB, and PD-L1 were overall not associated with consistent differences across lung cancer histological subtypes (Figures 4C and S3I–J).

We performed multivariate analyses to determine the clinical and molecular features that best correlate with CD39 expression on CD8⁺ T cells. We included tissue site, stage, histology, driver mutation, TMB, smoking history, and PD-L1 as potential covariates. We included HLA heterozygosity^{33,34} in the model and also

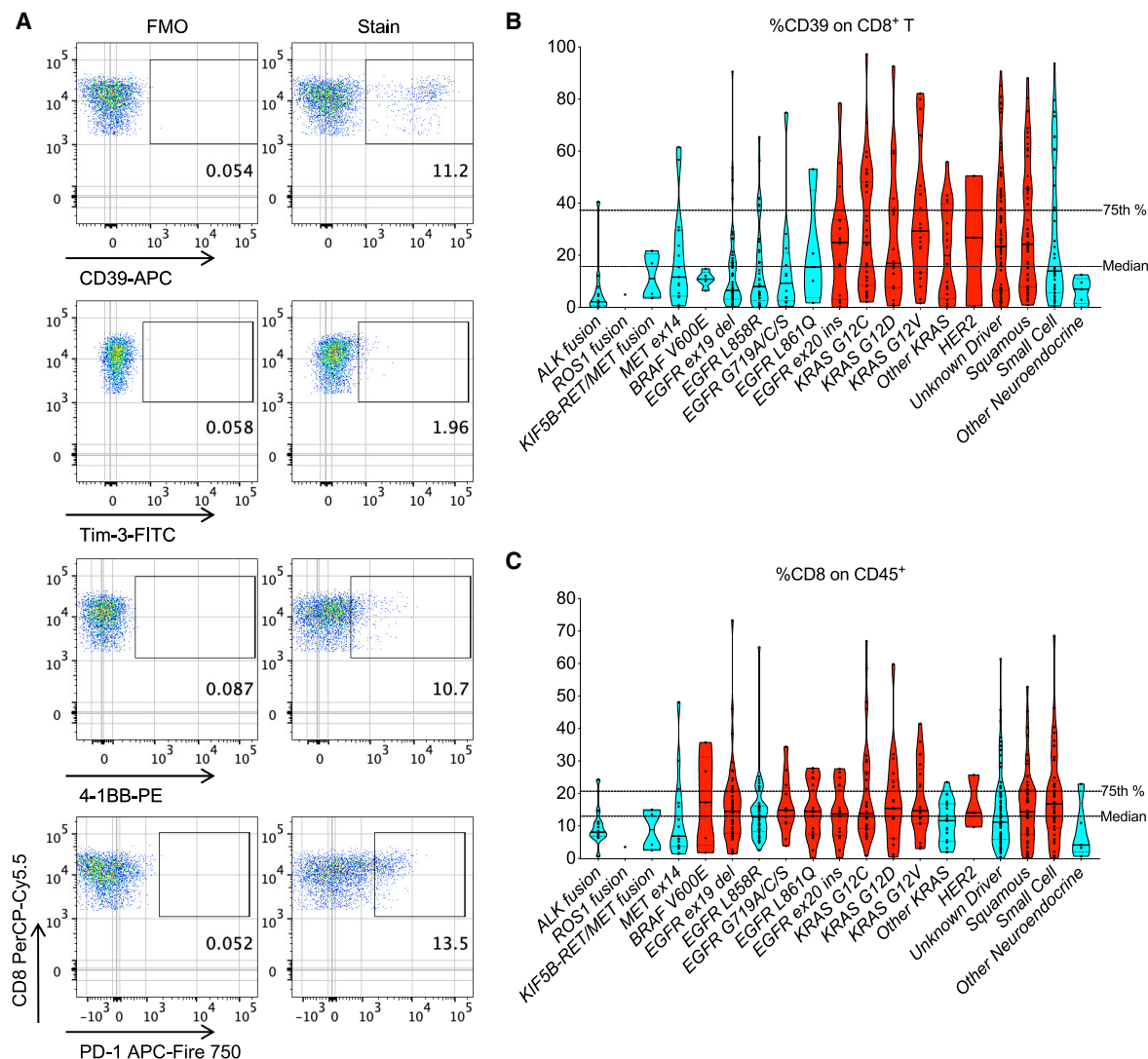


Figure 4. CD39 expression among intratumoral CD8⁺ T cells varies with lung cancer subtype

(A) Representative flow cytometry staining of CD39, Tim-3, 4-1BB, and PD-1 on DAPI⁻ CD45⁺ CD3⁺ CD8⁺ T cells from MSK 1105b. Left plot represents fluorescence minus one (FMO), and right plot represents the CD8⁺ T cells stained with the indicated antibody.

(B and C) Violin plots of %CD39⁺ (among CD8⁺ T cells) and %CD8⁺ (among CD45⁺) for various histological subtypes/driver mutation categories among the 440-sample cohort. Dashed lines indicate the median and 75th percentile CD39 level for entire 440-sample cohort. Red bars indicate histological subtypes/driver mutations with above median %CD39 values.

the number of predicted neoantigens and strong binding neoantigens from next-generation sequencing of tumor biopsies by MSK-IMPACT.³⁵ A linear model predicted the variance in % CD39 on CD8⁺ T cells at an adjusted R-squared of 0.24, which suggested that the features in the model poorly predict the variance observed in CD39 levels (Table S5C). In the model, only TMB, PD-L1, pericardial metastases, and prior chemotherapy passed significance thresholds of $p < 0.05$. Since some of the features in the dataset had few observations and in order to avoid overfitting, we also applied a lasso regression with 10-fold cross-validation. The lambda was selected based on the root-mean-square error (RMSE), and the model achieved an R-squared of 0.17 with a RMSE of 1.5 at lambda = 0.1 (Table S5D). At higher lambdas, the algorithm removed all pre-

dictors, which suggested that there was no linear combination of any regressed parameters that predicted CD39 levels well. Overall, these results indicate that CD39 expression on CD8⁺ T cells is a feature of the tumor that is non-redundant to the tumoral parameters that currently guide therapy in lung cancer (e.g., histology, driver alterations PD-L1, and TMB).

CD39 is upregulated on CD8⁺ T cells in the tumor microenvironment

We next examined the patterns of tissue-specific expression for CD39 and thus performed CD39 staining on CD8⁺ T cells from matched peripheral blood and tumor samples with varied anatomic sites (e.g., the brain, lymph node, and lung). In all three cases, CD39⁺ CD8⁺ T cells were preferentially observed in the

tumor tissue and not in the peripheral blood (Figure S4A). This was in agreement with our findings that CD8⁺ T cell interactions with cancer cells drive the expression of CD39 (Figure 3) and that CD39 is expressed at higher levels in regions of a resected tumor with viable cancer cells, compared with regions without viable tumor, normal adjacent regions, and lymph nodes.³⁶ Since there was a small CD39⁺ population of intermediate intensity in the peripheral blood, we evaluated whether this population gave rise to the CD39⁺ CD8⁺ T cells in the tumor tissue. To address this question, we sorted CD39⁻ and CD39⁺ CD8⁺ T cells from the peripheral blood and CD39⁻ or CD39⁺ from the tumor tissue. We then performed bulk TCR sequencing analysis and assessed for clonal overlap. As assessed by the Morisita index, there was minimal clonal overlap between CD39⁺ CD8⁺ T cells from the peripheral blood and CD39⁺ CD8⁺ T cells from tumor tissue, suggesting that circulating CD39⁺ CD8⁺ T cells may not be the dominant precursors for the CD39⁺ CD8⁺ T cells in the tumor microenvironment (Figures S4A–S4C).

Due the durability of CD39 expression (Figure 3; Chow et al.²⁵), we next assessed the robustness of CD39 levels across spatially and temporally distinct lesions. We analyzed 12 paired samples in which two anatomically distinct lesions were simultaneously assessed (e.g., two resected lung lesions, lymph node and primary lung lesions, or pleural metastasis and fluid). We noted reasonable concordance across spatially distinct lesions (Figure S4D), as exemplified by the low %CD39⁺ on CD8⁺ T cells from the paired pleural metastasis and fluid from MSK 1266 (Figure S4E). There was one case of divergent CD39 levels. MSK 1372a and b were simultaneous resections of two right-sided, separate primary lung cancer lesions with marked differences in CD39 expression (59.0% versus 92.5%; Figure S4F). Consistent with being separate primary lesions, these two tumors comprised two different *KRAS* driver mutations with differential levels of TMB, which may underlie the divergence of CD39 expression. We also followed %CD39⁺ on CD8⁺ T cells from the same anatomic site multiple times (e.g., recurrent pleural effusions, initial lung biopsy followed by resection, and serial resections for recurrent disease in the brain). The %CD39⁺ on CD8⁺ T cells across nine patients were largely durable over time, including for three brain lesions that were resected over the course of 9 months (MSK 1265; Figures S4G and S4H). These findings highlighted that %CD39⁺ on CD8⁺ T cells is increased in proximity to the tumor and that CD39 levels on CD8⁺ T cells are relatively preserved across spatially and temporally distinct lesions in the same patient.

PD-1/PD-L1 axis blockade increases the frequency of CD39⁺ CD8⁺ T cells

Since our data and prior reports^{11,15} demonstrate that tumor-antigen-reactive CD8⁺ T cells express CD39 in lung cancer, we sought to leverage CD39 as a proxy for anti-tumor CD8⁺ T cell immunosurveillance. Chemotherapy can result in “immunogenic cell death” that can prime an anti-tumor CD8⁺ T cell response.³⁷ We reasoned that %CD39⁺ on CD8⁺ T cells would be increased in patients after cytotoxic chemotherapy if such immune priming occurred. Analogously, ICB therapy expands the pool of antigen-specific CD8⁺ T cells that infiltrate the tumor,³⁸ which we reasoned might be reflected in increased CD39⁺ CD8⁺ T cells in the tumor. Thus, we evaluated in our dataset whether the

%CD39⁺ among CD8⁺ T cells increased with either cytotoxic chemotherapy and/or ICB therapy.

We first investigated the 218 patients in our cohort with stage-IV lung cancer who were treated with or without chemotherapy and/or ICB in the prior 3 or 6 months. Both total CD8⁺ infiltration and total %CD39⁺ on CD8⁺ T cells were unchanged in patients receiving cytotoxic chemotherapy in the preceding 3 or 6 months (Figures 5A–5D). Total CD8⁺ infiltration was also unchanged in patients receiving prior ICB therapy (Figures 5A and 5C). By contrast, CD8⁺ T cells from patients that received ICB in the prior 3 or 6 months expressed higher levels of CD39 (Figures 5B and 5D). In patients that received both cytotoxic chemotherapy and ICB therapy in the prior 3 or 6 months, %CD39⁺ on CD8⁺ T cells was unchanged, compared with patients that had not received chemotherapy or ICB, which is consistent with chemotherapy and ICB having opposing effects on CD39 expression (Figures 5B and 5D).

Since the stage IV lung cancer cohort is quite heterogeneous, we subsequently examined 208 early-stage (stages I–III) NSCLC biospecimens from patients that did or did not receive neoadjuvant therapy prior to sample collection. Among early-stage patients with NSCLC, we again did not observe differences in total CD8⁺ T cell infiltration with preceding neoadjuvant chemotherapy; however, neoadjuvant immunotherapy did increase total CD8⁺ T cell infiltration (Figure 5E). Patients who underwent neoadjuvant chemotherapy had reduced %CD39⁺ on CD8⁺ T cells, compared with patients without neoadjuvant therapy; by contrast, in patients who underwent neoadjuvant ICB, we observed an increase in CD39 expression on CD8⁺ T cells (Figure 5F). Thus, across two clinical cohorts, we did not find evidence for immunogenic cell death with standard cytotoxic chemotherapy utilized for lung cancer; however, we did discover that ICB exposure was associated with an enhanced infiltration of CD39⁺ CD8⁺ T cells. This is consistent with the concept that ICB results in clonal expansion and infiltration of tumor-reactive CD8⁺ T cells.³⁸

Since anti-tumor efficacy is associated with the development of immune-related adverse events (IRAEs) in patients treated with ICB (reviewed in Das et al.³⁹), we examined whether CD39 expression on CD8⁺ T cells was associated with IRAEs in our dataset. From our cohort of 440 patients treated with ICB, we performed a retrospective review for IRAEs. Among the patients with or without a history of IRAEs, there was no difference in incidence that was associated with total CD8⁺ T cell abundance, %CD39⁺ on CD8⁺ T cells, TMB, or PD-L1 (Figures S4I–S4L). This suggests that IRAE development is independent of the magnitude of tumor-reactive CD8⁺ T cells.

CD39 expression on CD8⁺ T cells portends benefit from ICB therapy

We next evaluated whether CD39 expression on CD8⁺ T cells had prognostic significance in our dataset. We first assessed 188 patients with the lung cancer stages from I to IIIA at the time of resection and correlated %CD39⁺ on CD8⁺ T cells with differential recurrence-free survival (RFS). Since CD39 expression was modulated by prior ICB (Figure 5F), we excluded patients who had previously received neoadjuvant ICB in this analysis. Across this early-stage resection cohort, we did not observe differences in RFS based on total CD8⁺ T cells or

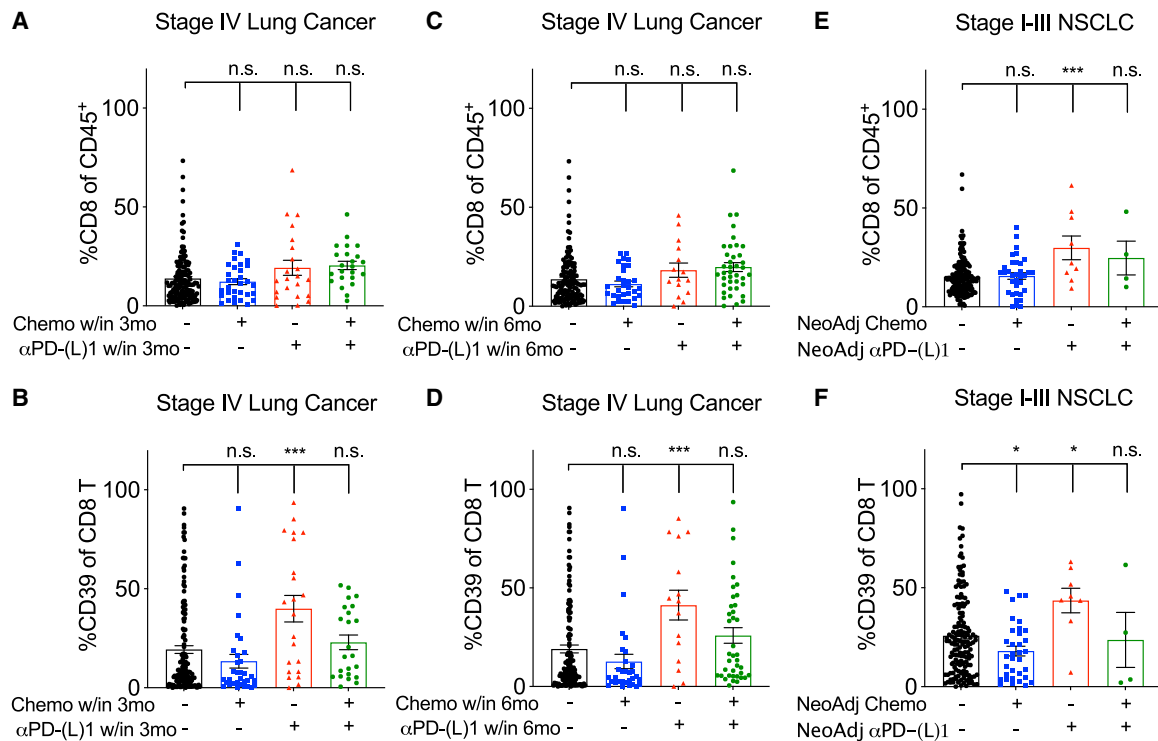


Figure 5. PD-1 axis blockade increases the frequency of CD39⁺ CD8⁺ tumor-infiltrating lymphocytes

(A and B) %CD8⁺ (among CD45⁺) or %CD39 (among CD8⁺ T cells) from 218 biospecimens obtained from patients with stage IV metastatic disease that did or did not receive chemotherapy or ICB therapy in the prior 3 months. Statistical significance was assessed by two-tailed Student's t test.

(C and D) %CD8⁺ (among CD45⁺) or %CD39 (among CD8⁺ T cells) from 218 biospecimens obtained from patients with stage IV metastatic disease that did or did not receive chemotherapy or ICB therapy in the prior 6 months. Statistical significance was assessed by two-tailed Student's t test.

(E and F) %CD8⁺ (among CD45⁺) or %CD39 (among CD8⁺ T cells) from 208 biospecimens obtained from patients with early stage (stages I–III) NSCLC. Error bars indicate SEM.

Statistical significance was assessed by two-tailed Student's t test. *p < 0.05 and ***p < 0.001.

%CD39⁺ among CD8⁺ T cells, utilizing the median or top quartile cutoff values from the total 440 patient dataset (Figures S5A–S5L). The data for CD8⁺ T cells are in line with a published prospective cohort of early-stage NSCLC resection specimens, which showed no differences in clinical outcomes based on total CD8⁺ T cell abundance.⁴⁰ Similarly, neither total CD8⁺ T cells or %CD39⁺ among CD8⁺ T cells resulted in differential progression-free survival (PFS) in the 26 stage IV lung cancer patients undergoing cytotoxic chemotherapy without ICB (Figures S5M–S5P). Hence, CD39 expression on CD8⁺ T cells was not prognostic for lung cancer in our dataset.

We next asked whether we could find evidence that %CD39⁺ on CD8⁺ T cells was associated with response to ICB. There were 23 patients in our cohort from whom we obtained baseline clinical biospecimens (defined as prior to or within 3 weeks of commencing ICB therapy) (Figure 6A; Table S5E). Although the tumoral PD-L1, TMB, and %CD8⁺ were not different between non-responders (stable disease/progression of disease) and responders (partial response) to ICB, we observed that responders had higher %CD39⁺ on CD8⁺ T cells (Figures 6B–6E). While total CD8⁺ infiltration did not differentiate PFS in these patients (Figures 6F and S5Q), patients with higher %CD39⁺ on CD8⁺ T cells had an improved PFS (Figures 6G and S5R). Responders also had higher PD-1

staining intensity on CD8⁺ T cells, and above median PD-1 expression on CD8⁺ T cells was associated with improved PFS (Figures S5S and S5T).

To further validate that baseline abundance of CD39⁺ CD8⁺ T cells was associated with clinical benefit from ICB, we derived a 23-gene signature score of CD39⁺ CD8⁺ T cells from our lung cancer single-cell dataset that included *ENTPD1*, *CXCL13*, *PDCD1*, and *ZNF683* (Table S3). We utilized this gene signature score to evaluate whether this was predictive of benefit from ICB in a dataset of baseline tumor transcriptomes of patients with NSCLC who were randomized to docetaxel chemotherapy or atezolizumab ICB in the phase III OAK clinical trial.^{41,42} We observed that patients receiving atezolizumab with above median or top quartile expression of the CD39⁺ CD8⁺ T cell signature had a longer PFS and overall (OS), compared with those with below median or bottom 75% level of the gene expression signature, respectively (Figures 6H–6K and S6A–S6D). This improvement in survival was not observed in the patients who were treated with docetaxel, which again indicates that baseline CD39⁺ CD8⁺ T infiltration is not prognostic in lung cancer. The predictive value of the CD39⁺ CD8⁺ T cell signature was also assessed in a multivariate model including a general T cell signature (*TBX21*, *ITK*, *CD3D*, *CD3E*, *CD3G*, *TRAC*, *TRBC1*, *TRBC2*, *CD28*, *CD5*, and *TRAT1*).⁴³ The signature score for CD39⁺

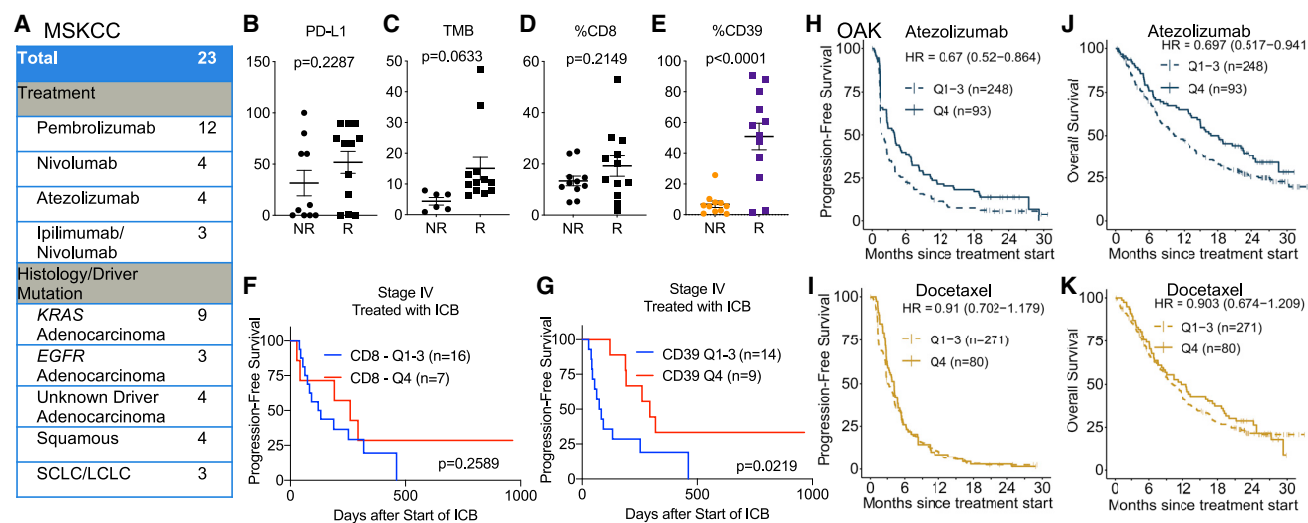


Figure 6. Baseline intratumoral CD39⁺ CD8⁺ T cells portends improved outcomes from immune checkpoint blockade in lung cancer

(A) Cohort of patients with stage IV lung cancer at MSKCC who received ICB monotherapy. SCLC, small cell lung cancer; LCLC, large cell lung cancer. (B–E) Tumor proportion score for PD-L1, tumor mutation burden, %CD8⁺ (among CD45⁺), and %CD39 (among CD8⁺ T cells) among non-responders (NR) and responders (R) to ICB in the cohort described in (A). Error bars indicate SEM. Statistical significance was determined by Mantel-Cox test.

(F and G) Kaplan-Meier survival curve of progression-free survival for patients described in cohort (A), based on stratification for top quartile (Q4) or bottom 75% level (Q1–Q3) of CD8⁺ T cells (F) and CD39 on CD8⁺ T cells (G).

(H–K) Progression-free and overall survival of patients with stage IV lung cancer in the phase III OAK clinical trial who were randomized to treatment with atezolizumab (H and J) or docetaxel (I and K). The patients were stratified by top quartile (Q4) or bottom 75% level (Q1–Q3) of a signature score for CD39⁺ CD8⁺ T cells.

CD8⁺ T cells trended toward significance (hazard ratio, HR = 0.72 [confidence interval, CI 0.50–1.04], p value = 0.077) in the atezolizumab arm of OAK, but no effect was seen in the docetaxel arm (HR = 1.12 [CI 0.76–1.66], p = 0.56), suggesting that the previous results may be specific and independent of total T cell infiltration (Figures S6E and S6F). Thus, the abundance of baseline “exhausted” CD8⁺ T cells was associated with clinical benefit from ICB therapy.

DISCUSSION

Lung cancer therapy is currently guided by tumor cell-intrinsic features, including histology, driver alterations, PD-L1, and TMB. Integration of tumor cell-extrinsic features such as the immune infiltrate can potentially lead to improved therapeutic options for patients with lung cancer. This is exemplified by the “lung cancer activation module”—consisting of activated T cells, plasma cells, and macrophages—that is a predictor of response to immunotherapy.⁴⁴ Since CD8⁺ T lymphocytes are the critical effectors in ICB therapy, features of these cells can also potentially serve as a non-redundant biomarker of response to ICB. Although methods to empirically verify tumor reactivity have improved substantially in sensitivity and throughput (e.g., MANA-FEST⁴⁵ and 4-1BB assay¹⁶), there remains a need in certain contexts for simple proxies to distinguish and quantify the tumor-reactive CD8⁺ T cell subpopulation from bystanders without cognate TCR reactivity. We observed from single-cell profiling of heterogeneous lesions that CD8⁺ T cells expressing high levels of CD39 were enriched for features of exhaustion, tumor reactivity, and clonal expansion. We empirically verified with TCR cloning of CD8⁺ T cells that CD39 enriched for tumor

reactivity. This is consistent with prior reports in melanoma, head and neck cancer,¹² and lung cancer,¹⁸ demonstrating that CD39 can be utilized to identify tumor-reactive T cells. While our manuscript did not examine the role of CD39 on CD4⁺ T cells, Hanada and colleagues demonstrated in four patients with lung cancer that 45% of CD8⁺ T cells and 66% of CD4⁺ T cells with a combination of protein CD39 and transcript *CXCL13* expression were neoantigen reactive.¹⁸ Hence, protein CD39 can be leveraged to “pan” for tumor-reactive TCRs and facilitate TCR discovery for adoptive T cell therapies.

Motivated by these findings and reports that tumor-reactive CD8⁺ T cells express CD39,^{2,11,12,15,16,18,21} we profiled CD39 expression on CD8⁺ T cells from 440 lung cancer biospecimens obtained at MSKCC. We observed that CD39 on CD8⁺ T cells is expressed more highly in tobacco-associated lung cancer genotypes and poorly correlates with TMB and tumoral PD-L1. Hence, CD39 is a biomarker that is non-redundant to tumoral features of lung cancer. %CD39⁺ on CD8⁺ T cells is likely dependent on other variables not captured in our dataset, including native T cell repertoire, HLA subtype, peptide binding, and likely the intersection of these three highly diverse attributes. CD39 expression increases on CD8⁺ T cells in the tumor microenvironment in response to secondary encounter with the tumor antigen and is generally stable across space and time. Finally, we demonstrate that although %CD39⁺ on CD8⁺ T cells was not prognostic in any of the patient cohorts that we examined, it was associated with clinical benefit, but not IRAEs, from ICB therapy. This suggests that the tumor-reactive CD39⁺ CD8⁺ T cells that exert immune pressure in the microenvironments are infrequently the same clones that mediate IRAEs in lung cancer.

There have been conflicting data regarding whether the presence of CD8⁺ T cells expressing markers of exhaustion can predict clinical benefit from ICB. Single-cell RNA-seq of tumors from metastatic melanoma revealed that a CD8⁺ T cell state called CD8⁺_B, which is enriched in *ENTPD1*, *PDCD1*, *CD38*, *HAVCR2*, and *LAG3*, is preferentially expressed in non-responders to ICB.⁸ Also, the use of multiplex immunofluorescence staining in lung cancer suggests that an “effector burnt out” (EBO) CD8⁺ T effector population preferentially expressing PD-1 and LAG-3, but not CD39, was enriched in patients who did not derive durable benefit from ICB and that these patients had reduced overall survival.⁴⁶ On the other hand, lung cancer patients with high pre-treatment levels of PD-1, by flow cytometry or immunofluorescence, demonstrated a greater response rate and PFS.^{2,47} Moreover, high levels of intratumoral CD39⁺ CD8⁺ T cells is associated with response to ICB therapy in lung cancer.⁴⁸ These findings dovetail with other studies that revealed that high levels of CD8⁺ T cells with features of exhaustion prior to ICB are associated with improved clinical benefit in colorectal cancer and ER⁺ breast cancer.^{49,50} Our data demonstrate that PD-1 and CD39 expression on CD8⁺ T cells are both predictive of improved outcomes from ICB therapy in lung cancer.

Limitations of the study

There are several limitations of this study that we acknowledge. First, the primary CD39 expression data were derived from patients treated at a single center. Second, while we profiled CD39 on CD8⁺ T cells, our data did not capture the likely contribution/modulation of other immune cell types such as CD4⁺ T cells, B cells, innate lymphoid cells, and myeloid cells. Lastly, our cohort to assess the predictive significance of CD39 expression on CD8⁺ T cells from patients with stage IV lung cancer treated with ICB monotherapy was limited to 23 patients despite >3 years of fresh tissue collection. Part of this limited sample size is attributable to the routine incorporation of cytotoxic chemotherapy to ICB for frontline treatment of the majority of patients with lung cancer. Due to the limited size of this cohort, we combined pre-treatment and early-on treatment (within 3 weeks of the start of ICB) as baseline samples, which may merge biologically distinct samples. By utilizing a gene signature of CD39⁺ CD8⁺ T cells to differentiate outcomes in a phase III clinical trial of lung cancer patients randomized to ICB or chemotherapy, we were able to orthogonally validate the results from this relatively small cohort. Despite these limitations, the data presented here contribute to our understanding of CD39 on CD8⁺ T cells in the context of lung cancer, including factors that modulate its pattern of expression. Our study identified CD39 on CD8⁺ T cells as a biomarker that is non-redundant to TMB and PD-L1 and that can be captured on clinical samples to serve as a proxy of the tumor-reactive CD8⁺ T cell population. Subsequent studies can also leverage CD39 to enrich for TCR candidates from CD8⁺ T cells to evaluate for TCR-based immunotherapies.

STAR★METHODS

Detailed methods are provided in the online version of this paper and include the following:

- KEY RESOURCES TABLE
- RESOURCE AVAILABILITY
 - Lead contact
 - Materials availability
 - Data and code availability
- EXPERIMENTAL MODEL AND SUBJECT DETAILS
 - Human biospecimens
 - Cell lines
 - Co-culture of NY-ESO1-reactive T cells with cognate antigen
- METHOD DETAILS
 - Single-cell transcriptome sequencing
 - Single-cell TCR (V(D)J) analysis from RNA
 - Cell surface protein feature barcode analysis
 - Single cell CITE/RNA/TCR analysis
 - Empiric testing of TCR reactivity
 - Flow cytometry
 - Bulk TCR sequencing of CD39⁻ and CD39⁺ populations
 - Immune-related adverse events annotation
 - Clinical outcomes analyses
- QUANTIFICATION AND STATISTICAL ANALYSIS
 - Multivariate analyses
 - Statistical analysis

SUPPLEMENTAL INFORMATION

Supplemental information can be found online at <https://doi.org/10.1016/j.immuni.2022.12.001>.

ACKNOWLEDGMENTS

We are grateful for experimental support from the MSKCC Molecular Cytology Core Facility, Flow Cytometry Core Facility, and Integrated Genomics Operation Core (funded by the NCI Cancer Center Support Grant [CCSG, P30 CA08748], Cycle for Survival, and the Marie-Josée and Henry R. Kravis Center for Molecular Oncology). We are grateful for manuscript editing provided by Dr. Clare Wilhelm and Reeja Thomas. This research was funded in part through the NIH NCI CCSG P30 CA008748, NCI R01 CA056821, U24 CA213274, P01 CA129243, R01 CA197936, R37 CA259177 (to C.A.K.), Cancer Research Institute CRI3176 (to C.A.K.), Stony Wold Herbert Fund, International Association of Lung Cancer Research (IASLC)/International Lung Cancer Foundation (ILCF), the MSKCC Society Grant, the Ludwig Collaborative and Swim Across America Laboratory, the Emerald Foundation, the Parker Institute for Cancer Immunotherapy at MSKCC, the Department of Medicine at MSKCC, Stand Up To Cancer (SU2C)-American Cancer Society Lung Cancer Dream Team Translational research grant (SU2C-AACR-DT17-15), Mark Foundation for Cancer Research (grant #19-029-MIA), Kay Stafford Fund, and Gibbons Scatone Family Foundation. A.C. was supported by an MSKCC Investigational Cancer Therapeutics Training Program fellowship (T32 CA-009207) and Clinical Investigator Award from the National Cancer Institute (K08 CA-248723).

AUTHOR CONTRIBUTIONS

A.C. conceived the project, performed experiments, analyzed the data, and wrote the manuscript in collaboration with the co-authors. F.Z.U., M.L., and A.D. performed experiments and analyzed data. B.Y.N., L.M., Y.L., H.R., S.T., J.E., S.S.C., A.F., A.H., X.G., and G.H. analyzed data. A.Q.-V., J.M.C., N.S., V.A., P.M., M.Mattar, M.Meneses, R.L., M.Ward, A.K., C.K., M.Wierzbicki, and J.Y. coordinated, procured, and processed human biospecimens. H.S., M.C., and D.H. performed experiments. J.M.-S. and M.S. provided critical reagents and methods. A.L.R., C.A.K., M.D.H., T.S., and E.d.S. supervised portions of the study. J.D.W., T.M., and C.M.R. conceived the project, wrote the manuscript, and supervised the study.

DECLARATION OF INTERESTS

C.A.K. received research funding support from Kite/Gilead and Intima Bioscience; is on the Scientific and/or Clinical Advisory Boards of Achilles Therapeutics, Aleta BioTherapeutics, Bellicum Pharmaceuticals, Catamaran Bio, Obsidian Therapeutics, and T-knife; and has performed consulting services for Bristol Myers Squibb, PACT Pharma, and Roche/Genentech. C.A.K. is a co-inventor on patent applications related to TCRs targeting public neoantigens unrelated to the current work. M.D.H. received a research grant from BMS; personal fees from Achilles, Arcus, AstraZeneca, Blueprint, BMS, Genentech/Roche, Genzyme, Immunai, Instil Bio, Janssen, Merck, Mirati, Natera, Nektar, Pact Pharma, Regeneron, Shattuck Labs, and Syndax; and equity options from Arcus, Factorial, Immunai, and Shattuck Labs. A patent filed by MSKCC related to the use of tumor mutational burden to predict response to immunotherapy (PCT/US2015/062208) is pending and licensed by PGDX. J.D.W. is a consultant for Amgen, Apricity, Ascentage Pharma, Astellas, AstraZeneca, Bicara Therapeutics, Boehringer Ingelheim, Bristol Myers Squibb, CellCarta, Chugai, Daiichi Sankyo, Dragonfly, Georgiamune, Idera, Imvaq, Larkspur, Maverick Therapeutics, Merck, Psioxus, Recepta, Tizona, Trishula, Sellas, Surface Oncology, and Werewolf Therapeutics. J.D.W. receives grant/research support from Bristol Myers Squibb and Sephora. J.D.W. has equity in Apricity, Arsenal IO, Ascentage, Beigene, Imvaq, Lineaues, Georgiamune, Maverick, Tizona Pharmaceuticals, and Trieza. J.D.W. is a co-inventor on the following patent application: xenogeneic (canine) DNA vaccines, myeloid-derived suppressor cell (MDSC) assay, anti-PD1 antibody, anti-CTLA4 antibodies, anti-GITR antibodies and methods of use thereof, Newcastle disease viruses for cancer therapy, and prediction of responsiveness to treatment with immunomodulatory therapeutics and method of monitoring abscopal effects during such treatment. J.D.W. and T.M. are co-inventors on patent applications related to CD40 and *in situ* vaccination (PCT/US2016/045970). T.M. is a consultant for Immunos Therapeutics and Pfizer. T.M. is a cofounder of and equity holder in IMVAQ Therapeutics. T.M. receives research funding from Bristol Myers Squibb, Surface Oncology, Kyn Therapeutics, Infinity Pharmaceuticals, Peregrine Pharmaceuticals, Adaptive Biotechnologies, Leap Therapeutics, and Aprea Therapeutics. T.M. is an inventor on patent applications related to work on oncolytic viral therapy, alpha virus-based vaccine, neoantigen modeling, CD40, GITR, OX40, PD-1, and CTLA-4. C.M.R. has consulted regarding oncology drug development with AbbVie, Amgen, Ascentage, AstraZeneca, BMS, Celgene, Daiichi Sankyo, Genentech/Roche, Ipsen, Loxo, and PharmaMar and is on the scientific advisory boards of Elucida, Bridge, and Harpoon. B.Y.N. and X.G. are employees and stockholders of Genentech/Roche.

Received: January 5, 2022

Revised: September 16, 2022

Accepted: December 2, 2022

Published: December 26, 2022

REFERENCES

- Ribas, A., and Wolchok, J.D. (2018). Cancer immunotherapy using checkpoint blockade. *Science* 359, 1350–1355. <https://doi.org/10.1126/science.aar4060>.
- Thommen, D.S., Koelzer, V.H., Hertzog, P., Roller, A., Trefny, M., Dimeloe, S., Kialainen, A., Hanhart, J., Schill, C., Hess, C., et al. (2018). A transcriptionally and functionally distinct PD-1(+) CD8(+) T cell pool with predictive potential in non-small-cell lung cancer treated with PD-1 blockade. *Nat. Med.* 24, 994–1004. <https://doi.org/10.1038/s41591-018-0057-z>.
- Hellmann, M.D., Ciuleanu, T.E., Pluzanski, A., Lee, J.S., Otterson, G.A., Audigier-Valette, C., Minenza, E., Linardou, H., Burgers, S., Salman, P., et al. (2018). Nivolumab plus ipilimumab in lung cancer with a high tumor mutational burden. *N. Engl. J. Med.* 378, 2093–2104. <https://doi.org/10.1056/NEJMoa1801946>.
- Reck, M., Rodríguez-Abreu, D., Robinson, A.G., Hui, R., Csósz, T., Fülöp, A., Gottfried, M., Peled, N., Tafreshi, A., Cuffe, S., et al. (2016). Pembrolizumab versus Chemotherapy for PD-L1-Positive non-small-Cell Lung Cancer. *N. Engl. J. Med.* 375, 1823–1833. <https://doi.org/10.1056/NEJMoa1606774>.
- Riaz, N., Havel, J.J., Makarov, V., Desrichard, A., Urba, W.J., Sims, J.S., Hodi, F.S., Martín-Algarra, S., Mandal, R., Sharfman, W.H., et al. (2017). Tumor and microenvironment evolution during immunotherapy with nivolumab. *Cell* 171, 934–949. <https://doi.org/10.1016/j.cell.2017.09.028>.
- Verma, V., Shrimali, R.K., Ahmad, S., Dai, W., Wang, H., Lu, S., Nandre, R., Gaur, P., Lopez, J., Sade-Feldman, M., et al. (2019). PD-1 blockade in subprimed CD8 cells induces dysfunctional PD-1(+)CD38(hi) cells and anti-PD-1 resistance. *Nat. Immunol.* 20, 1231–1243. <https://doi.org/10.1038/s41590-019-0441-y>.
- Helmink, B.A., Reddy, S.M., Gao, J., Zhang, S., Basar, R., Thakur, R., Yizhak, K., Sade-Feldman, M., Blando, J., Han, G., et al. (2020). B cells and tertiary lymphoid structures promote immunotherapy response. *Nature* 577, 549–555. <https://doi.org/10.1038/s41586-019-1922-8>.
- Sade-Feldman, M., Yizhak, K., Bjorgaard, S.L., Ray, J.P., de Boer, C.G., Jenkins, R.W., Lieb, D.J., Chen, J.H., Frederick, D.T., Barzily-Rokni, M., et al. (2018). Defining T cell states associated with response to checkpoint immunotherapy in melanoma. *Cell* 175, 998–1013. <https://doi.org/10.1016/j.cell.2018.10.038>.
- Osorio, J.C., Arbour, K.C., Le, D.T., Durham, J.N., Plodkowski, A.J., Halpenny, D.F., Ginsberg, M.S., Sawan, P., Crompton, J.G., Yu, H.A., et al. (2019). Lesion-level response dynamics to programmed cell death protein (PD-1) blockade. *J. Clin. Oncol.* 37, 3546–3555. <https://doi.org/10.1200/JCO.19.00709>.
- Scheper, W., Kelderman, S., Fanchi, L.F., Linnemann, C., Bendle, G., de Rooij, M.A.J., Hirt, C., Mezzadra, R., Slagter, M., Dijkstra, K., et al. (2019). Low and variable tumor reactivity of the intratumoral TCR repertoire in human cancers. *Nat. Med.* 25, 89–94. <https://doi.org/10.1038/s41591-018-0266-5>.
- Simoni, Y., Becht, E., Fehlings, M., Loh, C.Y., Koo, S.L., Teng, K.W.W., Yeong, J.P.S., Nahar, R., Zhang, T., Kared, H., et al. (2018). Bystander CD8(+) T cells are abundant and phenotypically distinct in human tumour infiltrates. *Nature* 557, 575–579. <https://doi.org/10.1038/s41586-018-0130-2>.
- Duhen, T., Duhon, R., Montler, R., Moses, J., Moudgil, T., de Miranda, N.F., Goodall, C.P., Blair, T.C., Fox, B.A., McDermott, J.E., et al. (2018). Co-expression of CD39 and CD103 identifies tumor-reactive CD8 T cells in human solid tumors. *Nat. Commun.* 9, 2724. <https://doi.org/10.1038/s41467-018-05072-0>.
- Li, H., van der Leun, A.M., Yofe, I., Lubling, Y., Gelbard-Solodkin, D., van Akkooi, A.C.J., van den Braber, M., Rozeman, E.A., Haanen, J.B.A.G., Blank, C.U., et al. (2019). Dysfunctional CD8 T cells form a proliferative, dynamically regulated compartment within human melanoma. *Cell* 176, 775–789. <https://doi.org/10.1016/j.cell.2018.11.043>.
- Yost, K.E., Satpathy, A.T., Wells, D.K., Qi, Y., Wang, C., Kageyama, R., McNamara, K.L., Granja, J.M., Sarin, K.Y., Brown, R.A., et al. (2019). Clonal replacement of tumor-specific T cells following PD-1 blockade. *Nat. Med.* 25, 1251–1259. <https://doi.org/10.1038/s41591-019-0522-3>.
- Caushi, J.X., Zhang, J., Ji, Z., Vaghiasa, A., Zhang, B., Hsiue, E.H., Mog, B.J., Hou, W., Justesen, S., Blosser, R., et al. (2021). Transcriptional programs of neoantigen-specific TIL in anti-PD-1-treated lung cancers. *Nature* 596, 126–132. <https://doi.org/10.1038/s41586-021-03752-4>.
- Oliveira, G., Stromhaug, K., Kläeger, S., Kula, T., Frederick, D.T., Le, P.M., Forman, J., Huang, T., Li, S., Zhang, W., et al. (2021). Phenotype, specificity and avidity of antitumour CD8(+) T cells in melanoma. *Nature* 596, 119–125. <https://doi.org/10.1038/s41586-021-03704-y>.
- Lowery, F.J., Krishna, S., Yossef, R., Parikh, N.B., Chatani, P.D., Zacharakis, N., Parkhurst, M.R., Levin, N., Sindiri, S., Sachs, A., et al. (2022). Molecular signatures of antitumor neoantigen-reactive T cells from metastatic human cancers. *Science* 375, 877–884.
- Hanada, K.I., Zhao, C., Gil-Hoyos, R., Gartner, J.J., Chow-Parmer, C., Lowery, F.J., Krishna, S., Prickett, T.D., Kivitz, S., Parkhurst, M.R., et al. (2022). A phenotypic signature that identifies neoantigen-reactive T cells in fresh human lung cancers. *Cancer Cell* 40, 479–493. <https://doi.org/10.1016/j.ccell.2022.03.012>.

19. Stoeckius, M., Hafemeister, C., Stephenson, W., Houck-Loomis, B., Chattopadhyay, P.K., Swerdlow, H., Satija, R., and Smibert, P. (2017). Simultaneous epitope and transcriptome measurement in single cells. *Nat. Methods* **14**, 865–868.
20. Gohil, S.H., Iorgulescu, J.B., Braun, D.A., Keskin, D.B., and Livak, K.J. (2021). Applying high-dimensional single-cell technologies to the analysis of cancer immunotherapy. *Nat. Rev. Clin. Oncol.* **18**, 244–256. <https://doi.org/10.1038/s41571-020-00449-x>.
21. van der Leun, A.M., Thommen, D.S., and Schumacher, T.N. (2020). CD8(+) T cell states in human cancer: insights from single-cell analysis. *Nat. Rev. Cancer* **20**, 218–232. <https://doi.org/10.1038/s41568-019-0235-4>.
22. Guo, X., Zhang, Y., Zheng, L., Zheng, C., Song, J., Zhang, Q., Kang, B., Liu, Z., Jin, L., Xing, R., et al. (2018). Global characterization of T cells in non-small-cell lung cancer by single-cell sequencing. *Nat. Med.* **24**, 978–985. <https://doi.org/10.1038/s41038-018-0045-3>.
23. Gueguen, P., Metoikidou, C., Dupic, T., Lawand, M., Goudot, C., Baulande, S., Lameiras, S., Lantz, O., Girard, N., Seguin-Givelet, A., et al. (2021). Contribution of resident and circulating precursors to tumor-infiltrating CD8(+) T cell populations in lung cancer. *Sci. Immunol.* **6**, eabd5778. <https://doi.org/10.1126/sciimmunol.abd5778>.
24. Miller, B.C., Sen, D.R., Al Abosy, R., Bi, K., Virkud, Y.V., LaFleur, M.W., Yates, K.B., Lako, A., Felt, K., Naik, G.S., et al. (2019). Subsets of exhausted CD8(+) T cells differentially mediate tumor control and respond to checkpoint blockade. *Nat. Immunol.* **20**, 326–336. <https://doi.org/10.1038/s41590-019-0312-6>.
25. Chow, A., Schad, S., Green, M.D., Hellmann, M.D., Allaj, V., Ceglia, N., Zago, G., Shah, N.S., Sharma, S.K., Mattar, M., et al. (2021). Tim-4(+) cavity-resident macrophages impair anti-tumor CD8(+) T cell immunity. *Cancer Cell* **39**, 973–988.e9. <https://doi.org/10.1016/j.ccell.2021.05.006>.
26. Zehn, D., Lee, S.Y., and Bevan, M.J. (2009). Complete but curtailed T-cell response to very low-affinity antigen. *Nature* **458**, 211–214. <https://doi.org/10.1038/nature07657>.
27. Ishihara, M., Kitano, S., Kageyama, S., Miyahara, Y., Yamamoto, N., Kato, H., Mishima, H., Hattori, H., Funakoshi, T., Kojima, T., et al. (2022). NY-ESO-1-specific redirected T cells with endogenous TCR knockdown mediate tumor response and cytokine release syndrome. *J. Immunother. Cancer* **10**, e003811. <https://doi.org/10.1136/jitc-2021-003811>.
28. Chakravarty, D., Gao, J., Phillips, S.M., Kundra, R., Zhang, H., Wang, J., Rudolph, J.E., Yaeger, R., Soumerai, T., Nissan, M.H., et al. (2017). OncoKB: A precision oncology knowledge base. *JCO Precis. Oncol.* **2017**. PO.17.00011. <https://doi.org/10.1200/PO.17.00011>.
29. Horn, L., Mansfield, A.S., Szczyńska, A., Havel, L., Krzakowski, M., Hochmair, M.J., Huemer, F., Losonczy, G., Johnson, M.L., Nishio, M., et al. (2018). First-line atezolizumab plus chemotherapy in extensive-stage small-cell lung cancer. *N. Engl. J. Med.* **379**, 2220–2229. <https://doi.org/10.1056/NEJMoa1809064>.
30. Paz-Ares, L., Dvorkin, M., Chen, Y., Reinmuth, N., Hotta, K., Trukhin, D., Staschenko, G., Hochmair, M.J., Özgüroğlu, M., Ji, J.H., et al. (2019). Durvalumab plus platinum-etoposide versus platinum-etoposide in first-line treatment of extensive-stage small-cell lung cancer (Caspian): a randomised, controlled, open-label, phase 3 trial. *Lancet* **394**, 1929–1939. [https://doi.org/10.1016/S0140-6736\(19\)32222-6](https://doi.org/10.1016/S0140-6736(19)32222-6).
31. Nguyen, E.M., Taniguchi, H., Chan, J.M., Zhan, Y.A., Chen, X., Qiu, J., de Stanchina, E., Allaj, V., Shah, N.S., Uddin, F., et al. (2022). Targeting lysine-specific demethylase 1 rescues major histocompatibility complex Class I antigen presentation and overcomes programmed death-ligand 1 blockade resistance in SCLC. *J. Thorac. Oncol.* **17**, 1014–1031. <https://doi.org/10.1016/j.jtho.2022.05.014>.
32. Burr, M.L., Sparbier, C.E., Chan, K.L., Chan, Y.C., Kersbergen, A., Lam, E.Y.N., Azidis-Yates, E., Vassiliadis, D., Bell, C.C., Gilan, O., et al. (2019). An evolutionarily conserved function of Polycomb silences the MHC Class I antigen presentation pathway and enables immune evasion in cancer. *Cancer Cell* **36**, 385–401.e8. <https://doi.org/10.1016/j.ccell.2019.08.008>.
33. Chowell, D., Krishna, C., Pierini, F., Makarov, V., Rizvi, N.A., Kuo, F., Morris, L.G.T., Riaz, N., Lenz, T.L., and Chan, T.A. (2019). Evolutionary divergence of HLA class I genotype impacts efficacy of cancer immunotherapy. *Nat. Med.* **25**, 1715–1720. <https://doi.org/10.1038/s41591-019-0639-4>.
34. Chowell, D., Morris, L.G.T., Grigg, C.M., Weber, J.K., Samstein, R.M., Makarov, V., Kuo, F., Kendall, S.M., Requena, D., Riaz, N., et al. (2018). Patient HLA class I genotype influences cancer response to checkpoint blockade immunotherapy. *Science* **359**, 582–587. <https://doi.org/10.1126/science.aao4572>.
35. Zehir, A., Benayed, R., Shah, R.H., Syed, A., Middha, S., Kim, H.R., Srinivasan, P., Gao, J., Chakravarty, D., Devlin, S.M., et al. (2017). Mutational landscape of metastatic cancer revealed from prospective clinical sequencing of 10,000 patients. *Nat. Med.* **23**, 703–713. <https://doi.org/10.1038/nm.4333>.
36. Pai, J.A., Chow, A., Sauter, J.L., Mattar, M., Rizvi, H., Woo, H.J., Shah, N., Uddin, F., Quintanal-Villalonga, A., Chan, J.M., et al. (2021). Regional and clonal T cell dynamics at single cell resolution in immune checkpoint blockade. Preprint at bioRxiv. 2021.2009.2027.461389.
37. Galluzzi, L., Buqué, A., Kepp, O., Zitvogel, L., and Kroemer, G. (2017). Immunogenic cell death in cancer and infectious disease. *Nat. Rev. Immunol.* **17**, 97–111. <https://doi.org/10.1038/nri.2016.107>.
38. Yost, K.E., Chang, H.Y., and Satpathy, A.T. (2021). Recruiting T cells in cancer immunotherapy. *Science* **372**, 130–131. <https://doi.org/10.1126/science.abd1329>.
39. Das, S., and Johnson, D.B. (2019). Immune-related adverse events and anti-tumor efficacy of immune checkpoint inhibitors. *J. Immunother. Cancer* **7**, 306. <https://doi.org/10.1186/s40425-019-0805-8>.
40. Federico, L., McGrail, D.J., Bentebibel, S.E., Haymaker, C., Ravelli, A., Forget, M.A., Karpinet, T., Jiang, P., Reuben, A., Negro, M.V., et al. (2022). Distinct tumor-infiltrating lymphocyte landscapes are associated with clinical outcomes in localized non-small cell lung cancer. *Ann. Oncol.* **33**, 42–56. <https://doi.org/10.1016/j.annonc.2021.09.021>.
41. Mazieres, J., Rittmeyer, A., Gadgeel, S., Hida, T., Gandara, D.R., Cortinovis, D.L., Barlesi, F., Yu, W., Matheny, C., Ballinger, M., and Park, K. (2021). Atezolizumab versus docetaxel in pretreated patients with NSCLC: final results from the randomized Phase 2 Poplar and Phase 3 OAK clinical trials. *J. Thorac. Oncol.* **16**, 140–150. <https://doi.org/10.1016/j.jtho.2020.09.022>.
42. Patil, N.S., Nabet, B.Y., Müller, S., Koeppen, H., Zou, W., Giltne, J., Au-Yeung, A., Srivats, S., Cheng, J.H., Takahashi, C., et al. (2022). Intratumoral plasma cells predict outcomes to PD-L1 blockade in non-small cell lung cancer. *Cancer Cell* **40**, 289–300.e4. <https://doi.org/10.1016/j.ccell.2022.02.002>.
43. Bagaev, A., Kotlov, N., Nomic, K., Svekolkin, V., Gafurov, A., Isaeva, O., Osokin, N., Kozlov, I., Frenkel, F., Gancharova, O., et al. (2021). Conserved pan-cancer microenvironment subtypes predict response to immunotherapy. *Cancer Cell* **39**, 845–865.e7. <https://doi.org/10.1016/j.ccell.2021.04.014>.
44. Leader, A.M., Grout, J.A., Maier, B.B., Nabet, B.Y., Park, M.D., Tabachnikova, A., Chang, C., Walker, L., Lansky, A., Le Berichel, J., et al. (2021). Single-cell analysis of human non-small cell lung cancer lesions refines tumor classification and patient stratification. *Cancer Cell* **39**, 1594–1609.e12. <https://doi.org/10.1016/j.ccell.2021.10.009>.
45. Danilova, L., Anagnostou, V., Caushi, J.X., Sidhom, J.W., Guo, H., Chan, H.Y., Suri, P., Tam, A., Zhang, J., Asmar, M.E., et al. (2018). The mutation-associated neoantigen functional expansion of specific T cells (MANAFEST) assay: A sensitive platform for monitoring antitumor immunity. *Cancer Immunol. Res.* **6**, 888–899. <https://doi.org/10.1158/2326-6066.CIR-18-0129>.
46. Sanmamed, M.F., Nie, X., Desai, S.S., Villareal-Espindola, F., Badri, T., Zhao, D., Kim, A.W., Ji, L., Zhang, T., Quinlan, E., et al. (2021). A burned-out CD8+ T-cell subset expands in the tumor microenvironment and curbs cancer immunotherapy. *Cancer Discov.* **11**, 1700–1715. <https://doi.org/10.1158/2159-8290.CD-20-0962>.

47. Kumagai, S., Togashi, Y., Kamada, T., Sugiyama, E., Nishinakamura, H., Takeuchi, Y., Vitaly, K., Itahashi, K., Maeda, Y., Matsui, S., et al. (2020). The PD-1 expression balance between effector and regulatory T cells predicts the clinical efficacy of PD-1 blockade therapies. *Nat. Immunol.* *21*, 1346–1358. <https://doi.org/10.1038/s41590-020-0769-3>.
48. Yeong, J., Suteja, L., Simoni, Y., Lau, K.W., Tan, A.C., Li, H.H., Lim, S., Loh, J.H., Wee, F.Y.T., Nerurkar, S.N., et al. (2021). Intratumoral CD39(+) CD8(+) T cells predict response to programmed cell death Protein-1 or programmed death Ligand-1 blockade in patients with NSCLC. *J. Thorac. Oncol.* *16*, 1349–1358. <https://doi.org/10.1016/j.jtho.2021.04.016>.
49. Chalabi, M., Fanchi, L.F., Dijkstra, K.K., Van den Berg, J.G., Aalbers, A.G., Sikorska, K., Lopez-Yurda, M., Grootsholten, C., Beets, G.L., Snaebjornsson, P., et al. (2020). Neoadjuvant immunotherapy leads to pathological responses in MMR-proficient and MMR-deficient early-stage colon cancers. *Nat. Med.* *26*, 566–576. <https://doi.org/10.1038/s41591-020-0805-8>.
50. Terranova-Barberio, M., Pawlowska, N., Dhawan, M., Moasser, M., Chien, A.J., Melisko, M.E., Rugo, H., Rahimi, R., Deal, T., Daud, A., et al. (2020). Exhausted T cell signature predicts immunotherapy response in ER-positive breast cancer. *Nat. Commun.* *11*, 3584. <https://doi.org/10.1038/s41467-020-17414-y>.
51. Wohlhieter, C.A., Richards, A.L., Uddin, F., Hulton, C.H., Quintanal-Villalonga, A., Martin, A., de Stanchina, E., Bhanot, U., Asher, M., Shah, N.S., et al. (2020). Concurrent mutations in STK11 and KEAP1 promote ferroptosis protection and SCD1 dependence in lung cancer. *Cell Rep.* *33*, 108444. <https://doi.org/10.1016/j.celrep.2020.108444>.
52. Gros, A., Parkhurst, M.R., Tran, E., Pasetto, A., Robbins, P.F., Ilyas, S., Prickett, T.D., Gartner, J.J., Crystal, J.S., Roberts, I.M., et al. (2016). Prospective identification of neoantigen-specific lymphocytes in the peripheral blood of melanoma patients. *Nat. Med.* *22*, 433–438. <https://doi.org/10.1038/nm.4051>.
53. Gallardo, H.F., Tan, C., Ory, D., and Sadelain, M. (1997). Recombinant retroviruses pseudotyped with the vesicular stomatitis virus G glycoprotein mediate both stable gene transfer and pseudotransduction in human peripheral blood lymphocytes. *Blood* *90*, 952–957.
54. Ghani, K., Wang, X., de Campos-Lima, P.O., Olszewska, M., Kamen, A., Rivière, I., and Caruso, M. (2009). Efficient human hematopoietic cell transduction using RD114- and GALV-pseudotyped retroviral vectors produced in suspension and serum-free media. *Hum. Gene Ther.* *20*, 966–974. <https://doi.org/10.1089/hum.2009.001>.
55. Rivière, I., Brose, K., and Mulligan, R.C. (1995). Effects of retroviral vector design on expression of human adenosine deaminase in murine bone marrow transplant recipients engrafted with genetically modified cells. *Proc. Natl. Acad. Sci. USA* *92*, 6733–6737. <https://doi.org/10.1073/pnas.92.15.6733>.
56. Eyquem, J., Mansilla-Soto, J., Giavridis, T., van der Stegen, S.J., Hamieh, M., Cunanan, K.M., Odak, A., Gönen, M., and Sadelain, M. (2017). Targeting a CAR to the TRAC locus with CRISPR/Cas9 enhances tumour rejection. *Nature* *543*, 113–117. <https://doi.org/10.1038/nature21405>.
57. Wu, F., Fan, J., He, Y., Xiong, A., Yu, J., Li, Y., Zhang, Y., Zhao, W., Zhou, F., Li, W., et al. (2021). Single-cell profiling of tumor heterogeneity and the microenvironment in advanced non-small cell lung cancer. *Nat. Commun.* *12*, 2540. <https://doi.org/10.1038/s41467-021-22801-0>.
58. Kuhn, M. (2008). Building Predictive Models in R Using the caret Package. *J. Stat. Software* *28*, 1–26. <https://doi.org/10.18637/jss.v028.i05>.
59. Friedman, J., Hastie, T., and Tibshirani, R. (2010). Regularization paths for generalized linear models via coordinate descent. *J. Stat. Softw.* *33*, 1–22.

STAR★METHODS

KEY RESOURCES TABLE

REAGENT or RESOURCE	SOURCE	IDENTIFIER
Antibodies		
CD45-BV510	Biolegend	Cat# 368526, RRID:AB_2687377
CD3-BV650	Biolegend	Cat# 304044, RRID:AB_2563812
CD8 ⁺ -PerCP-Cy5.5	Biolegend	Cat# 344710, RRID:AB_2044010
CD8 ⁺ -BV510	Biolegend	Cat# 344732, RRID:AB_2564624
EGFR-PE/Cy7	Biolegend	Cat# 352909, RRID:AB_2562158
4-1BB-PE	Biolegend	Cat# 309804, RRID:AB_31478
PD-1-APC/Fire 750	Biolegend	Cat# 329954, RRID:AB_2616721
PD-1-PerCP/Cy5.5	Biolegend	Cat# 329914, RRID:AB_1595461
CD39-APC	Biolegend	Cat# 328210, RRID:AB_1953234
CD39-PE/Cy7	Biolegend	Cat# 328212, RRID:AB_2099950
CD4-Alexa Fluor 700	Biolegend	Cat# 357418, RRID:AB_2616933
Human TruStain FcX™, BioLegend, Human TruStain FcX™ Blocking Buffer	Biolegend	Cat# 422302, RRID:AB_2818986
TotalSeq(TM)-C Human Universal Cocktail, V1.0	Biolegend	Cat# 399905, RRID:AB_2876728
TotalSeq™-C0251 anti-human Hashtag 1 Antibody	Biolegend	Cat# 394661, RRID:AB_2801031
TotalSeq™-C0252 anti-human Hashtag 2 Antibody	Biolegend	Cat# 394663, RRID:AB_2801032
TotalSeq™-C0253 anti-human Hashtag 3 Antibody	Biolegend	Cat# 394665, RRID:AB_2801033
TotalSeq™-C0254 anti-human Hashtag 4 Antibody	Biolegend	Cat# 394667, RRID:AB_2801034
TotalSeq™-C0255 anti-human Hashtag 5 Antibody	Biolegend	Cat# 394669, RRID:AB_2801035
Anti-MHC I	BioXCell	Cat# BE0079, RRID:AB_1107730
Bacterial and virus strains		
One Shot™ Stbl3™ Chemically Competent E. coli	ThermoFisher Scientific	Cat# C737303
NY-ESO1-GFP Lentiviral Plasmids	SinoBiological	Cat# HG15611-ACGLN
Biological samples		
Tumor tissue from NSCLC patients	Resection, biopsy and effusion biospecimens from patients with informed consent at Memorial Sloan Kettering Cancer Center.	This study
MSK 1087 PDX	MSKCC Rudin Lab	This study
MSK 1111 PDX	MSKCC Rudin Lab	This study
Healthy donor PBMCs	New York Blood Center	Leukopheresis pack
NY-ESO1-reactive T cells (donor 401)	Charles River	Cat# ASTC-1093
Chemicals, peptides, and recombinant proteins		
RPMI	Corning	Cat# 10-041-CV
Human serum	Gemini Biosciences	Cat# 100-512-100
Penicillin/streptomycin	Gibco	Cat# 15140122
Amphotericin	Gibco	Cat# 15290026
Glutamax	Gibco	Cat# 35050061
Minimum essential amino acids	Millipore Sigma	Cat# M7145

(Continued on next page)

Continued

REAGENT or RESOURCE	SOURCE	IDENTIFIER
Sodium pyruvate	Gibco	Cat# 11360070
Tumor Dissociation Kit, human	Miltenyi	Cat# 130-095-929
Polybrene	Sigma	Cat# TR-1003-G
Retro-X Concentrator	Takara	Cat# 631455
Retronectin GMP grade	Takara	Cat# T202
EasySep™ Human CD8 ⁺ T Cell Isolation Kit	Stem Cell Technologies	Cat# 17953
DNase I Solution (1 mg/mL)	Stem Cell Technologies	Cat# 100-0762
IL-2	Peprotech	Cat# 200-02
IL-15	Peprotech	Cat# 200-15
IFN γ	Peprotech	Cat# 300-02
Cell Trace Violet	Invitrogen	Cat# C34557
Dynabeads™ Human T-Activator CD3/CD28 for T Cell Expansion and Activation	Invitrogen	Cat# 11132D
Bambanker Serum Free Cell Freezing Medium	VWR	Cat# 101974-112
Dapi, for nucleic acid staining	Sigma-Aldrich	Cat# D9542-50MG

Critical commercial assays

NEBuilder® HiFi DNA Assembly Cloning Kit	New England BioLabs	Cat# E5520S
Chromium Chip A	10X Genomics	Cat# PN-230027
Next GEM Chip K	10X Genomics	Cat# PN-1000286
Chromium Single Cell 5' Reagent Kit	10X Genomics	Cat# PN-1000006
Next GEM Single Cell 5' Kit v2	10X Genomics	Cat# PN-1000263
Chromium Single Cell V(D)J Enrichment Kit Human T Cell	10X Genomics	Cat# PN-1000005
Chromium Single Cell 5' Feature Barcode Library Kit	10X Genomics	Cat# PN-1000080
NovaSeq 6000 SP Reagent Kit v1.5	Illumina	Cat# 20028401
NovaSeq 6000 S1 Reagent Kit v1.5	Illumina	Cat# 20028319
NovaSeq 6000 S4 Reagent Kit v1.5	Illumina	Cat# 20028312
NovaSeq 6000 S2 Reagent Kit v1.5	Illumina	Cat# 20028316
aMPure XP beads	Beckman Coulter	Cat# A63882
4D-Nucleofector	Lonza	Cat# V4XP-3024
Sanger Sequencing	Azenta Life Sciences	Custom
AllPrep DNA/RNA Mini Kits	Qiagen	Cat# 80204

Deposited data

Single cell CITE/RNA/TCRseq of MSK 1087, 1111, 1222, and 1256	NCBI GEO	GSE218262
Bulk TCR sequencing of MSK 1265b, 1322a, and 1336a	Adaptive Biotechnologies ImmuneAccess	https://doi.org/10.21417/AC20221
Raw and processed RNA-seq data from OAK	European Genome-phenome Archive	EGAS00001005013
Relevant clinical data from OAK	European Genome-phenome Archive	EGAS00001005013

Experimental models: Cell lines

H522	ATCC	RRID:CVCL_1567
H522-NY-ESO1	This paper	N/A
293T H29 packaging cell line	MSKCC Sadelain Lab	REF ⁵¹
293T RD114-envelope cell line	MSKCC Sadelain Lab	REF ⁵²

(Continued on next page)

Continued

REAGENT or RESOURCE	SOURCE	IDENTIFIER
Oligonucleotides		
Cas9 RNP	QB3 UC Berkley Macrolab Facility	Cas9-NLS purified protein
Human TRAC gRNA	Synthego	CRISPRRevolution sgRNA EZ Kit, custom-made (sequence in text)
Human TRBC gRNA	Synthego	CRISPRRevolution sgRNA EZ Kit, custom-made (sequence in text)
G block fragments for TCR cloning	IDT	Custom-made (sequences in Table S5)
Recombinant DNA		
SFG retroviral plasmid with EGFRt marker	MSKCC Sadelain Lab	This study
Software and algorithms		
FlowJo	TreeStar	Version 10.8.1
Prism	Graphpad	Version 9.0.0
Seurat	https://github.com/satijalab/seurat	Version 3.1.1
CellRanger	10X Genomics	Version 3.1.0
Caret R package	https://CRAN.R-project.org/package=caret	Version 6.0-93

RESOURCE AVAILABILITY**Lead contact**

Further information and requests will be fulfilled by the lead contact, Charles M. Rudin (rudinc@mskcc.org).

Materials availability

PDX lines from MSK 1087 and 1111 are available and can be requested from the [lead contact](#).

Data and code availability

Single cell data for lung cancer biospecimens are uploaded to NIH GEO: GSE218262. Bulk TCR sequencing data are uploaded to Adaptive Biotechnologies Immunoseq database (immune ACCESS <https://doi.org/10.21417/AC20221>).

EXPERIMENTAL MODEL AND SUBJECT DETAILS**Human biospecimens**

Fresh primary tumors, metastatic lesions and pleural/peritoneal/pericardial effusions were obtained from August 2018 to September 2021 with permission from the MSKCC IRB. Informed consent was collected from all patients enrolled in this study. Clinical samples were annotated with tumor histology and driver mutation. Adenocarcinoma, adenocarcinoma, and NSCLC NOS tumors were annotated by their molecular driver mutations, if known. The category 'Unknown Driver' refers to adenocarcinoma, adenocarcinoma, and NSCLC NOS histology tumors for which a driver mutation (defined as 'known to be oncogenic' by OncoKB²⁸) was not identified; notably, this category does not include squamous or small cell histology biospecimens. With the exception of a single case in which a tumor sample with squamous histology harbored a *MET* exon 14 mutation and two transformed small-cell lung cancer tumors with *EGFR* mutations, squamous and small-cell lung cancers were annotated by their histology.

Cell lines

A cell line could be derived from the MSK 1111 PDX and was maintained in RPMI supplemented with 10% human serum, 1% penicillin/streptomycin, 0.1% amphotericin, 1X GlutaMax, 1mM sodium pyruvate, and 1X minimum essential amino acids (complete media). The PDX from MSK 1087 could not be propagated in cell culture and cryopreserved PDX cells (>80% human EPCAM⁺) were utilized immediately after thawing. Virus-producing cell lines (H29 and RD114-envelope producers) were previously described.^{53,54} H522 cell line was maintained in complete media. H522-NY-ESO1 was generated by transduction with NY-ESO1-GFP lentiviral plasmids lentiviral particles. Lentiviral production and transduction were performed as previously described.⁵¹ GFP⁺ cells were flow-sorted (BD Aria) and expanded prior to cryopreservation.

All cell lines were cultured in a 5% CO₂ incubator at 37°C and passaged every 2-3 days.

Co-culture of NY-ESO1-reactive T cells with cognate antigen

Cryopreserved healthy donor CD8⁺ T cells enriched for NY-ESO1-reactive T cells were obtained from Charles River. Notably, these cells were previously expanded *ex vivo* in the presence of NY-ESO1 peptide and cryopreserved prior to purchase. The certificate of analysis indicates that the cells were 98% viable with 73.74% of the cells were positive for staining with CD8⁺ and HLA-A*02:01-NY-ESO1 tetramer. These CD8⁺ T cells were labeled with 1 μM of Cell Trace Violet per manufacturer's instructions and then plated at 2.5×10^4 viable T cells per 100 μl of complete T cell media in a 24W plate in 'reservoir' wells.

1×10^5 irradiated (30Gy, Cesium source irradiator) H522 or H522-NYESO1 tumor cells were cultured for 24 hours with 10ng/ml of IFN γ and plated onto a 96W flat-bottom plate. On days 1, 4, 7, 8, 9, and 10 after this plating of the tumor cells, 100 μl of the CTV-labeled NY-ESO1-reactive T cells were added from the reservoir well to the respective co-culture well and flow cytometry (see below) was performed on day 11 after the initial tumor cell plating, which coincides with day 10, 7, 4, 3, 2, and 1 of T cell co-culture, respectively. CD8⁺ T cells from the reservoir well was utilized as a 'no co-culture' condition.

For the peptide-pulsed experiments, 1×10^5 irradiated H522 tumor cells were cultured for 24 hours with 10ng/ml of IFN γ and plated onto a 96W flat-bottom plate. On days 1, 4, 7, 9, and 10 after this plating of the tumor cells, 100 μl of the CTV-labeled NY-ESO1-reactive T cells were added from the reservoir well to the respective co-culture well and flow cytometry (see below) was performed on day 11 after the initial tumor cell plating, which coincides with day 10, 7, 4, 2, and 1 of T cell co-culture, respectively. CD8⁺ T cells from the reservoir well was utilized as a 'no co-culture' condition.

METHOD DETAILS

Single-cell transcriptome sequencing

Sorted or dissociated tumor cells were stained with Trypan blue and Countess II Automated Cell Counter (ThermoFisher) was used to assess both cell number and viability. Following QC, the single-cell suspension was loaded onto Chromium Chip A or Next GEM Chip K and GEM generation, cDNA synthesis, cDNA amplification, and library preparation of 700–3,300 cells proceeded using the Chromium Single Cell 5' Reagent Kit or Next GEM Single Cell 5' Kit v2 according to the manufacturer's protocol. cDNA amplification included 14–16 cycles and 5.8 ng–20 ng of the material was used to prepare sequencing libraries with 16 cycles of PCR. Indexed libraries were pooled equimolar and sequenced on a NovaSeq 6000 in a PE26/91 or PE28/91 run using the NovaSeq 6000 SP or S1 Reagent Kit. An average of 108 million reads were generated per sample.

Single-cell TCR (V(D)J) analysis from RNA

An aliquot of complementary DNA (cDNA) generated using the methods described above was used to enrich for V(D)J regions using the Chromium Single Cell V(D)J Enrichment Kit Human T Cell according to the manufacturer's protocol with 10 cycles of PCR during enrichment and 9 cycles during library preparation. Indexed libraries were pooled equimolar and sequenced on a NovaSeq 6000 in a PE150 or PE26/91 run using the NovaSeq 6000 SP or S4 Reagent Kit. An average of 24 million paired reads was generated per sample.

Cell surface protein feature barcode analysis

Amplification products generated using the methods described above included both cDNA and feature barcodes tagged with cell barcodes and unique molecular identifiers. Smaller feature barcode fragments were separated from longer amplified cDNA using a 0.6X cleanup with aMPure XP beads. Libraries were constructed using the Chromium Single Cell 5' Feature Barcode Library Kit according to the manufacturer's protocol with 9 cycles of PCR. Indexed libraries were pooled equimolar and sequenced on a NovaSeq 6000 in a PE26/91 or PE28/91 run using the NovaSeq 6000 SP or S2 Reagent Kit. An average of 60 million paired reads was generated per sample.

Single cell CITE/RNA/TCR analysis

Single-cell sequencing data were aligned to the Genome Reference Consortium Human Build 38 (GRCh38) using Cell Ranger in order to obtain T cell clonotypes, feature barcoding, CITEseq antibody detection and gene expression profiles associated with individual single cells. Each data type was matched to create a UMI matrix and cells were filtered out based on three metrics: (1) cells with fewer than 200 detectable genes; (2) cells with more than 3000 detectable genes; (3) cells that had fewer than 5% percentage of counts related to mitochondrial genes. Data normalization, Principal Component Analysis and subsequent Uniform Manifold Approximation and Projections (UMAP) were performed on the dataset using Seurat. The differential expression comparisons were generated using the DESeq2 package with selected genes. After filtering, we created subclusters of cells using the Louvain algorithm. Raw counts were normalized by library size per cell. CD39^{neg} was defined as a normalized value of 0 for *ad_t_CD39*. CD39^{int} was defined as the *ad_t_CD39* level between 0 and 1.0 (non-inclusive) since 1.0 was the mean of all non-zero values for *ad_t_CD39* among all the cells in the CD8⁺ cluster. CD39^{hi} was defined as *ad_t_CD39* level greater than or equal to 1.0. Signature scores for exhaustion, proliferation and tumor reactivity were calculated by *AddModuleScore* in Seurat. Clonal proportion was calculated as the fractional representation of all CD8⁺ clones by clonotypes that were categorized by mean *ad_t_CD39* expression with the same cutoffs for CD39^{neg}, CD39^{int}, and CD39^{hi} as above.

Empiric testing of TCR reactivity

TCR fragments for positive control NY-ESO1 TCR or candidate CD39^{hi}, CD39^{int}, and CD39^{neg} CD8⁺ T cell sequences (Table S5) were constructed as previously described.⁵² We joined the TRB and TRA chains (with human TRAC and TRBC chains) with a furin SGSG P2A linker, cloned the TCR constructs into an SFG γ -retroviral vector⁵⁵ and sequence-verified all plasmids with Sanger sequencing. We transfected retrovirus vectors into H29 cells using calcium phosphate to produce VSV-G pseudo-typed retroviruses.⁵³ We next used Polybrene and viral-containing supernatants to generate stable RD114-enveloped producer cell lines.⁵⁴ We collected and concentrated virus-containing supernatants using Retro-X™ Concentrator.

Deletion of endogenous TCR in healthy donor PBMC was achieved as previously described⁵⁶ with some modifications. CD8⁺ T cells from healthy donors were initially separated with negative selection for CD8⁺ T cells and cryopreserved in Bamberker media. CD8⁺ T cells were thawed and then incubated with DNase I for 20 minutes at 37°C and then activated for 48 hours with anti-CD3/CD28 Dynabeads. Activated CD8⁺ T cells were then electroporated with a Cas9 ribonucleoprotein and guide RNAs targeting the TRAC and TRBC sequences via 4D-Nucleofector. The electroporated CD8⁺ T cells were then rested overnight in complete media supplemented with IL-2 (240IU/ml) and IL-15 (10ng/ml) (complete T cell media). The guide RNA sequences utilized are as follows:

TRAC gRNA sequence

5'-C*A*G*GGUUCUGGAUAUCUGUGUUUUAGAGCUAGAAUAGCAAGUUAUUUUUAAAG

GCUAGUCCGUUAUCAACUUGAAAA AGUGGCACCGAGUCGGUGCU*U*U-3'

TRBC gRNA sequence

5'-GCAGUAUCUGGAGUCAUUGA-3'

Asterisk (*) represents 2'-O-methyl 3' phosphorothioate. Endogenous TCR deletion efficiency was >90%, as assessed by CD3 assessment in untransduced TRAC/TRBC-edited cells.

For T cell transductions, we coated non-tissue culture treated 24-well plates with Retronectin as per the manufacturer's protocol. We plated a 0.5x10⁶ activated electroporated T cells per well, and centrifuged cells for 1 hour at room temperature at 400g (acceleration 3, brake 0). Successfully transduced T cells were utilized in co-culture assays with matched tumor targets (H522-NYESO1, MSK 1087 PDX cells, or MSK 1111 PDX-derived cell line) between 7-10 days post transduction or cryopreserved for future use. In order to enhance MHC I expression, tumor targets were incubated with 10ng/ml of human IFN for 24 hours prior to addition of T cells.

1x10⁵ IFN γ -treated tumor targets were co-cultured with 1x10⁵ total T cells after transduction in a 96 well V bottom plate in complete T cell medium. 10 μ g/ml of anti-MHC I (clone W6/32) were added to some wells to assess for MHC I dependence. %4-1BB was evaluated by flow cytometry (see below) on EGFRt⁺ transduced CD8⁺ T cells. TCRs were considered reactive if the %4-1BB was \geq 5% higher in the well with PDX co-culture (without anti-MHC I) compared to the T cells alone.¹⁶

Flow cytometry

Cells were incubated with TruFCX to block nonspecific binding, and then stained (15 min, 4 °C) with appropriate dilutions of various combinations of fluorochrome-conjugated anti-human antibodies. The stained cells were acquired on a LSRII Flow Cytometer or BD Aria cell sorter and the data were processed using FlowJo software. Doublets and dead cells were excluded based on forward scatter (FSC) and side scatter (SSC) and 4',6-diamidino-2-phenylindole staining (DAPI, 1 μ g/ml). All depicted flow cytometry plots were gated on non-debris (by FSC and SSC), viable (DAPI⁺) single CD45⁺ CD3⁺ cells, unless otherwise indicated in the Figure legend. Gating for %4-1BB, %PD-1, and %CD39 was determined by gating of fluorescence minus one (FMO). PD-1 mean fluorescence intensity was measured for a subset of samples.

Bulk TCR sequencing of CD39⁻ and CD39⁺ populations

From MSK 1265b, 1322a, and 1336a, CD39⁻ and CD39⁺ CD8⁺ T cell populations were flow-sorted from the peripheral blood and tissues on a BD Aria cell sorter. Cell pellets were initially frozen at -80°C and then genomic DNA (gDNA) was extracted with the AllPrep DNA/RNA Mini kit. gDNA was then shipped to Adaptive Biotechnologies for bulk TCR sequencing.

Immune-related adverse events annotation

Patient charts were analyzed for the period from the start of immunotherapy treatment until six months after treatment. Physicians' notes and lab work were analyzed for identification of IRAE, including colitis, pneumonitis, hypothyroidism, arthralgias or other events and if the patient was treated with steroids. Patients with and without IRAE were assessed for a difference in CD39⁺ CD8⁺ T cell abundance, total CD8⁺ T cell infiltrate, TMB, or PD-L1 expression.

Clinical outcomes analyses

RFS assessment was performed on 188 biospecimens obtained from stage I-IIIa lung cancer who did not receive neoadjuvant ICB and were not lost to follow up after resection. For the PFS assessment in stage IV patients not treated with ICB, only patients that received at least two cycles of platinum-based chemotherapy were included in the analysis (n=26). For the PFS assessment in stage IV patient treated with ICB, only patients that received at least two cycles of ICB without chemotherapy were included in the analysis (n=23). The median cutoffs for %CD8⁺ among CD45⁺ and %CD39 among CD8⁺ of 13.0 and 15.7, respectively, and top quartile (Q4) cutoff of 20.6 and 37.23, respectively, were selected from the 440-sample cohort. The PD-1 cutoff of 750 was selected to divide the cohort above and below the median for the stage IV cohort. Response criteria were annotated per RECIST v1.1.

A gene expression signature suitable for estimation of CD39⁺ CD8⁺ T cells from bulk RNA-seq of NSCLC tumors was derived by first identifying genes that were differentially expressed by CD39^{hi} CD8⁺ T cells from the human scRNA-seq dataset. To eliminate signals from other cell types present in the tumor microenvironment, we filtered against independent NSCLC scRNA-seq data⁵⁷ to only select genes expressed in the T/NK cell compartment, as described previously.⁴² We further refined the signatures by selecting genes that were well correlated with *ENTPD1* (Spearman R >0.5) in bulk NSCLC tumor RNA-seq from the OAK clinical trial.⁴² Single sample gene signature scores were assigned to bulk RNA-seq samples from OAK by taking the median z-score of the genes that comprise the signature. Multivariate Cox models compared the association with survival of the signature score of CD39⁺ CD8⁺ T and a general T cell infiltration score (Table S4).

Progression-free survival was plotted for lung patients that were randomized and treated with atezolizumab or docetaxel chemotherapy on the Phase 3 OAK clinical trial.⁴¹ PFS curves were stratified by either the median expression or top quartile (Q4) vs bottom 3 quartiles (Q1-3) of expression of the CD39⁺ CD8⁺ T cell gene signature.

QUANTIFICATION AND STATISTICAL ANALYSIS

Multivariate analyses

We used the R package *caret*⁵⁸ to implement the *glmnet*⁵⁹ algorithm and evaluate the performance of a lasso regression model using 10-fold cross-validation. The data was centered and scaled during preprocessing and lambda was chosen based on the minimal RMSE value. Additionally, a linear model was evaluated using the R function “*lm*”. In both models, the response variable, CD39 expression, was log base 2 transformed as well as the predictor variables TMB and total neoantigens per sample.

Statistical analysis

Data are expressed and statistical analyses were performed as described in the Figure legend for each analysis. Statistical significance was determined by two-way ANOVA with Tukey's multiple comparison test, student's t test or Mantel-Cox log-rank test using Prism 7 software as indicated.